



Observations on soil-atmosphere interactions after long-term monitoring at two sample sites subjected to shallow landslides

M. Bordoni¹ · M. Bittelli² · R. Valentino³ · V. Vivaldi¹ · C. Meisina¹

Received: 5 March 2021 / Accepted: 12 June 2021 / Published online: 27 July 2021
© The Author(s) 2021

Abstract

Soil-atmosphere interaction has implications in different scientific research contexts and is increasingly investigated through field measurements. This paper reports a detailed description of interaction between shallow soil and atmosphere at two test sites in Oltrepò Pavese area (Northern Italy). The two test sites are in the same climatic area but are characterised by different geological features. In fact, the first objective is to compare the behaviour of two different soils, namely a clayey-sandy silt (CL) and a silty clay (CH), under similar meteorological events. Soil-atmosphere interaction is studied on the basis of long-term (about 87 and 42 months for the two test sites, respectively) monitoring data of both volumetric water content and soil water potential, recorded at different depths along two vertical soil profiles in the first two metres from ground level. Field measurements, together with meteorological data such as precipitation and air temperature, allow for clear identification of the seasonal fluctuations of unsaturated soil hydraulic properties. To infer detailed information, the recorded data were processed and relationships between soil water potential and water content were investigated. Different time spans, from several months to a few days, even including single rainy events, are considered to show the hydraulic soil behaviour. The hysteretic cycles of water content with respect to soil water potential and non-equilibrium flow are highlighted. In particular, the measured soil water potential is in the range of 0–800 kPa and of 0–1500 kPa for the CL and CH soil, respectively. At both sites, the observed hysteretic cycles are more frequent in the hot season (summer) than in the cold season (winter) and tend to reduce with depth. The experimental results are compared with the soil water characteristic curves (SWCCs) to assess whether and to what extent the SWCCs are reliable in modelling the hydraulic behaviour of partially saturated soils, under atmospheric forcing, at least in the considered climatic contexts.

Keywords Monitoring · Unsaturated soil · Water content · Water potential · Hydrological hysteresis

Introduction

Rainfall infiltration and water redistribution in unsaturated soils as well as the response of shallow soil to atmospheric forcing are natural phenomena that affect different aspects related to the fields of hydrology, geology, ecology and agronomy. In particular, under the geotechnical point of view, rainfall infiltration may cause unsaturated soils to fail

on shallow portions of both natural and artificial slopes. This is commonly due to a reduction of matric suction (or soil water potential) which is strictly linked to a reduction of shear strength. To investigate slope stability as well as improve quality of instability predictions, field monitoring of soil hydraulic characteristics is very important.

This research started from the analysis of the factors triggering rainfall-induced shallow landslides, but it is believed that the information acquired on soil-atmosphere interaction may be of much wider interest.

Recently, many researchers studied soil-atmosphere interactions related to slope stability problems through field monitoring in different geological and climate contexts, but very limited studies have been carried out in the area of the Apennine chain in northern Italy. In Europe, Smethurst et al. (2012) identified several physical processes in soil water content and pore-water pressure observed for six years in a

✉ M. Bordoni
massimiliano.bordoni@unipv.it

¹ Department of Earth and Environmental Sciences, University of Pavia, Pavia, Italy

² Department of Agricultural and Food Sciences, University of Bologna, Bologna, Italy

³ Department of Chemistry, Life Sciences and Environmental Sustainability, University of Parma, Parma, Italy

London Clay cutting near Newbury (UK); Papa et al. (2013) and Pirone et al. (2015a, 2015b) acquired seasonal field data in an unsaturated pyroclastic slope at Monteforte Irpino test site (southern Italy); Comegna et al. (2016a, b) and Marino et al. (2020) reported soil-atmosphere monitoring data collected in shallow deposits in unsaturated pyroclastic soils covering a steep slope located in Cervinara, southern Italy, where in 1999 a rainfall-induced flowslide occurred; Springman et al. (2013) reported results of a long-term field study related to water content and suction fluctuations in Quaternary soil deposits on a grass-covered slope in north Switzerland; Bittelli et al. (2012) studied seasonal variations of soil–water conditions leading to landslide occurrence in a high plasticity inorganic clay in the Centonara catchment (northern Italian Apennine). As for eastern Asia, Rahardjo and co-workers carried out dozens of field monitoring programs oriented to investigate variations in matric suction profiles on slopes with different boundary conditions in Singapore (Gasmo et al. 2000; Lim et al. 1996; Rahardjo et al. 2005, 2008, 2011); Leung et al. (2011, 2013a, 2013b) carried out field monitoring of water content, matric suction and seasonal movement of groundwater flow on unsaturated saprolitic hillslopes of Hong Kong islands prone to shallow landslides; in Japan, Watakabe and Matsushi (2019) identified the lithological and hydrological controls on the occurrence of shallow slope instabilities by means of a comprehensive field hydrological and meteorological monitoring. In USA, soil-moisture fluctuation was monitored in the unsaturated zone of different shallow colluvial landslides in Kentucky on the basis of water content, suction and electrical resistivity measurements (Crawford and Bryson 2018; Crawford et al. 2018, 2019); the United States Geological Survey (USGS) developed and implemented several test sites in different geological and geomorphological settings of the USA susceptible to shallow failures, in order to identify both predisposing and triggering conditions for early-warning system strategies (Godt et al. 2008, 2009; Mirus et al. 2017). Moreover, Ashland (2021) stressed on the combination between intense rainfall events, significant antecedent cumulated rainfall amounts and high level of initial soil water content leading to induce the triggering of multiple and widespread shallow landslides, giving important insights on anticipating future slope failure conditions.

In this framework, the present paper describes results of a field activity, based on a long-term monitoring of two test sites in two typical geological environments of Oltrepò Pavese (Northern Italy), where no similar studies have been carried out in the past. The selected test sites represent the typical slope settings prone to rainfall-induced shallow landslides in this area. At both sites, field monitoring of climatic conditions as well as extensive laboratory tests, and in situ measurements of volumetric water content and soil water potential (or pore-water pressure) at different depths in the first 2 m from ground

level were carried out. These hydraulic parameters are the main basic characteristics to be considered when assessing the hydraulic behaviour of a partially saturated soil in relation to rainfall events and are very useful as input data in different types of water balance models and slope stability analyses.

Field data considered herein span about 7 years at the first test site (Montuè) and 4 years at the second test site (Costa Cavalieri). They show that variations in water content and soil water potential are closely linked to the alternation of wetting and drying periods and are also very sensitive to isolated rainfalls. To infer detailed information on the soil behaviour at the two test sites, the recorded data have been processed and different relationships between soil water potential and water content have been obtained. Different time spans, even including single rainy events, are considered to show the hydraulic soil behaviour. The hysteretic cycles of water content with respect to soil water potential in the unsaturated soil behaviour are highlighted. Many authors recently focused on the same aspect, under the experimental point of view (Tami et al. 2004; Yang et al. 2012; Rianna et al. 2014; Pirone et al. 2014; Bovolenta et al. 2020; Liang 2020) or by proposing different solutions to model this natural phenomenon (Li 2005; Comegna et al. 2016b; Fredlund 2019; Chen et al. 2019; Wei et al. 2020). Bordoni et al. (2017) already investigated how to improve the estimation of complete field SWCCs based on field data acquired at Montuè test site on a time lapse of 5 years (Bordoni et al. 2015). In this paper, the first objective is showing field measurement series and related observations for a time lapse much longer than that presented in Bordoni et al. (2015) for one of the two test sites; the further objective is to compare the hydraulic soil behaviour of two different kinds of soils in the same climatic area. The experimental results are also compared with the soil water characteristic curves (SWCCs) to assess whether and to what extent the SWCCs are reliable in modelling the hydraulic behaviour of partially saturated soils, under atmospheric forcing, at least in the considered climatic contexts. This last aspect is treated under a twofold perspective with respect to other similar researches. First of all, the detailed monitoring of the hydraulic behaviour in different thin soil sub-layers aims at showing that it may not always be appropriate modelling the behaviour of a shallow soil in the first two meters from ground level using only a single SWCC, even though the soil appears homogeneous in terms of geotechnical characteristics (Comegna et al. 2016b; Fredlund 2019). Secondly, the data acquired in the field experimentally confirm what has been observed by other authors on the rain infiltration into the shallow soil, i.e. the extent to which this phenomenon is characterised by non-equilibrium and prevalent flow through preferential pathways, rather than a uniform water flow in a homogeneous medium, especially when the clay content is relatively high (Vogel et al. 2010; Diamantopoulos et al. 2012; Shao et al. 2015).

Data and methods

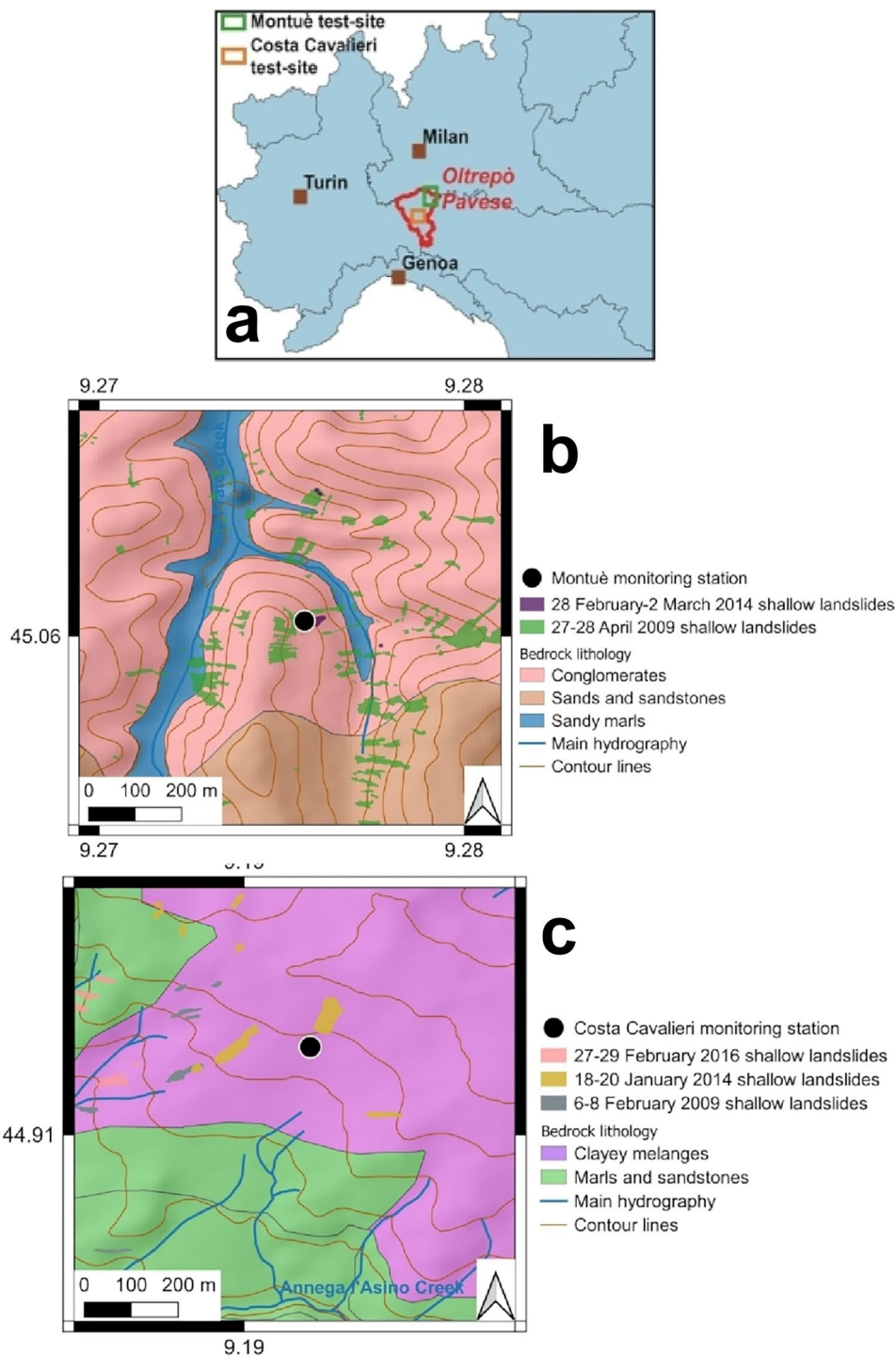
Montuè test site

One of the two selected test sites is located near the village of Montuè (Fig. 1b) in north-eastern Oltrepò Pavese (Scuropasso catchment). The bedrock is made of gravel, sand and poorly cemented conglomerates, with a low percentage of

marls. As regards the groundwater, deep water circulation is confined in fractured levels located at different depths in the bedrock, without forming a continuous aquifer (Vercesi and Scagni 1984).

The test site is faced towards east and is characterised by steep slopes (26° – 35°). The slope elevation ranges between 170 and 210 m a.s.l., and the monitoring station is located at 185 m. a.s.l. The land cover on the slope is

Fig. 1 Location of the test sites **a**, geomorphological and shallow landslides at Montuè **b** and Costa Cavalieri **c** test sites



mainly constituted by grass and shrubs, instead it becomes a woodland of black robust trees at slope toe.

According to Koppen's classification of world climates, the climatic regime is temperate/mesothermal (*Csa*: Mediterranean hot summer climate) with a mean yearly temperature of 12 °C and mean yearly rainfall around 700 mm (2004–2018 period).

The surrounding area is frequently affected by shallow landslides. In particular, when an extreme rainfall event (160 mm of cumulated rain in 62 h) caused many shallow landslides in the whole region of Oltrepò Pavese on 27–28 April 2009, this area was characterised by the highest shallow landslides density (29 landslides per km²) (Bordoni et al. 2015) (Fig. 1b). The selected test-slope was affected

by a further shallow failure that occurred between 28 February and 2 March 2014, as a consequence of a rainfall event of 68.9 mm in 42 h (Bordoni et al. 2015). The source areas of the observed shallow landslides were characterised by slope angles between 30° and 35°, and failure surfaces were at about 1 m below the slope surface.

Shallow landslides in this area involve superficial soils derived from bedrock weathering. They are prevalently clayey-sandy silts and clayey-silty sands. Different amounts of pebbles and carbonate concretions are also present. Three main soil levels can be identified in the sample site (Fig. 2a).

From the ground surface down to 0.7 m, the soil is characterised by a clayey-sandy silt texture with low plasticity, high content in carbonates as soft concretions, and unit weight in

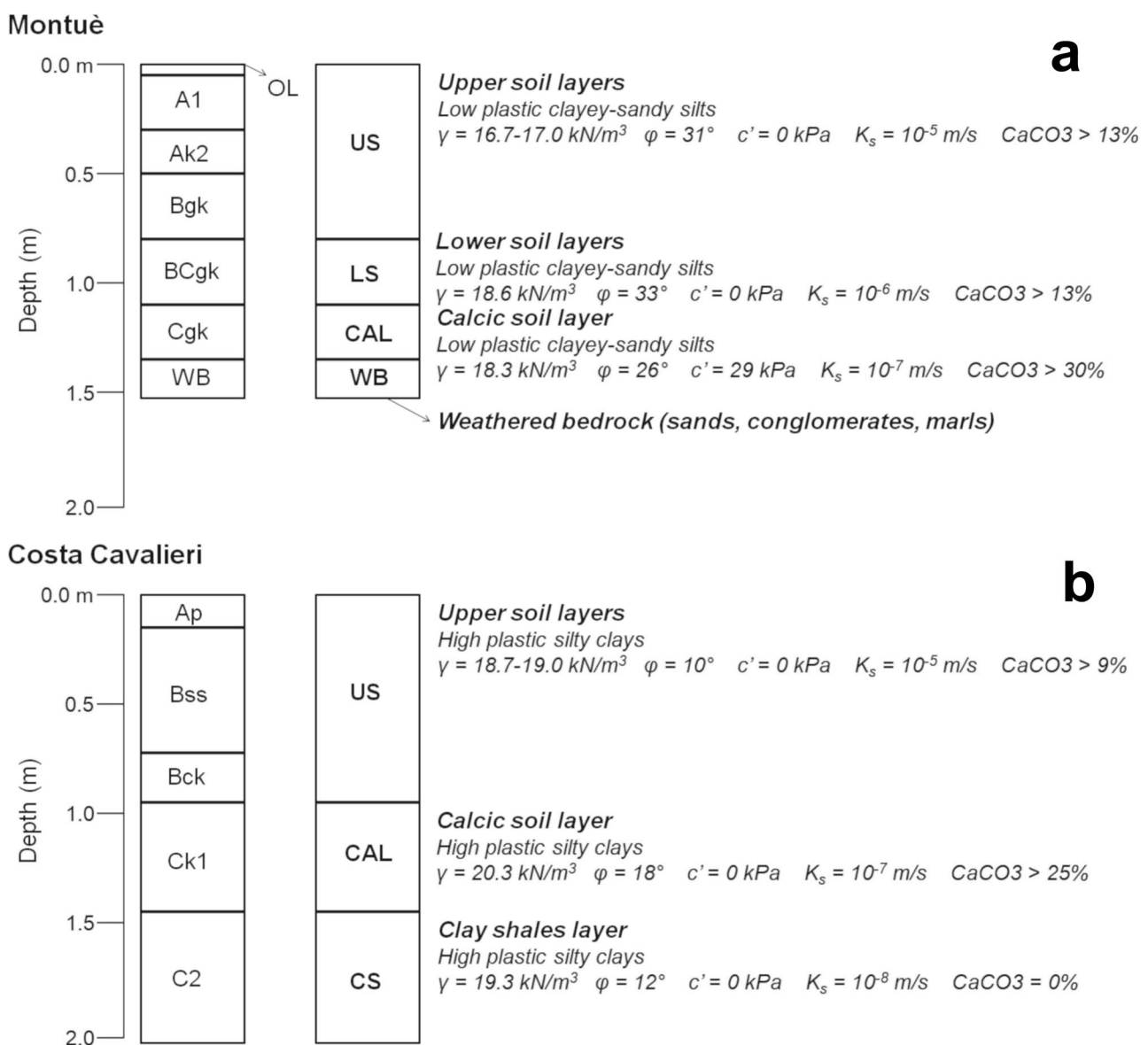


Fig. 2 Representative soil profiles of the test sites. **a** Montuè. **b** Costa Cavalieri

the order of 16.7–17.0 kN/m³. This level groups the upper soil layers (US) and includes the following pedological horizons: OL (0–0.01 m), A1 (0.01–0.1 m), Ak2 (0.1–0.2 m), Apgk3 and Bgk (0.4–0.7 m) (Fig. 2a).

A further soil layer (LS), corresponding to a pedological BCgk horizon, is characterised by similar texture, plasticity and carbonate content with respect to US, but with a higher unit weight of 18.6 kN/m³. This layer develops between 0.7 and 1.1 m from the ground level. At a depth between 1.1 and 1.3 m, the soil (Cgk horizon from the pedological point of view) has the same textural, plasticity and density features of the LS layer, but it is characterised by a significant increase in carbonate content up to 35.3%. This layer can be classified as a calcic horizon (CAL), where the carbonate concretions are more dense than in other levels. The weathered bedrock (WB), composed of sand and poorly cemented conglomerates, is positioned at 1.3 m below the ground surface.

The soil layers also have different mechanical and hydrological features. As regards the peak shear strength parameters, obtained through triaxial tests, US and LS are characterised by similar values of friction angle, equal to 31 and 33°, respectively, and by a nil effective cohesion. Instead, the CAL level has a lower value of the friction angle (26°), but a higher effective cohesion, equal to 29 kPa. Oedometric tests performed on undisturbed samples show that all soil layers are over-consolidated.

Saturated hydraulic conductivity, measured in the field through an amoozometer, decreases as depth increases. US has the highest value along the soil profile, in the order of 10⁻⁵ m/s, while LS and CAL are characterised by a saturated hydraulic conductivity equal to 10⁻⁶ m/s and 10⁻⁷ m/s, respectively.

Table 1 summarises the main soil features at Montuè test site.

Costa Cavalieri test site

The second test site is located near the village of Costa Cavalieri (Fig. 1c) in central Oltrepò Pavese (Ardivestra catchment). The bedrock is composed of a clayey melange, with

scattered calcareous and marly blocks, which can reach metric dimensions. Due to the very low permeability of these materials, the water table is at a depth of around 30–40 m from the slope surface, thus not affecting the phenomena in the shallow soil layers (Vercesi and Scagni 1984).

The test site is characterised by low-medium topographic gradient (7–18°) and is south western-facing. The slope elevation ranges from 460 to 500 m a.s.l., and the monitoring station is located at 468 m. a.s.l. A cultivation of alfalfa entirely covers the test site slope.

As for the Montuè test site, the climatic regime of Costa Cavalieri area is temperate/mesothermal (*Csa*: Mediterranean hot summer climate) according to Koppen's classification of world climates. The mean yearly temperature is 11 °C and the mean yearly rainfall depth is around 720 mm (2005–2018 period).

The area where the Costa Cavalieri test site is located is characterised by a high density of past shallow landslides (3 landslides per km², based on the events that occurred in 2009, 2014 and 2016; Fig. 1c). Field evidences suggest the occurrence of several phenomena, also in correspondence to the tested slope, since February 2009 (Fig. 1c). In particular, rainfall-induced shallow landslides were triggered in areas close to the monitored slope during the following events: 6–8 February 2009 (as a consequence of a rainfall of 54 mm in 65 h), 18–20 January 2014 (rainfall of 52 mm in 42 h) and 5–6 March 2016 (rainfall of 42.6 mm in 24 h). The source areas were characterised by a slope angle of about 16°, and failure surfaces were at 0.9 m from the ground level.

Silty clay layers involved in shallow landslides at this test site were derived by bedrock weathering. Three main soil layers can be identified (Fig. 2b), with different geotechnical, physical, mechanical and hydrological features with respect to those at Montuè test site.

From the ground surface down to 0.9 m, the soil is characterised by a silty clay texture with high plasticity, high content in carbonates as soft concretions, and unit weight in the order of 18.7–19.0 kN/m³. This level groups the upper soil layers (US), which correspond to the following horizons

Table 1 Main properties of soils at various levels at Montuè test site

Soil level	Depth m	Gravel %	Sand %	Silt %	Clay %	w _L %	P _I %	USCS class	γ kN/m ³	φ' °	c' kPa	CaCO ₃ %	K _s m/s
US	0.2	12.3	12.5	53.9	21.3	39.8	17.2	CL	17.0	31	0.0	14.1	10 ⁻⁵
	0.4	1.6	11.0	59.5	27.9	38.5	14.3	CL	16.7			15.7	
	0.6	8.5	13.2	51.1	27.2	40.3	15.7	CL	16.7			14.1	
LS	1.0	2.4	12.2	56.4	29.0	39.2	15.9	CL	18.6	33	0.0	16.1	10 ⁻⁶
CAL	1.2	0.5	7.5	65.6	26.4	41.8	16.5	CL	18.2	26	29.0	35.3	10 ⁻⁷
WB	1.4	0.2	75.0	24.8	0.0	-	-	SM	18.1	-	-	13.7	-

w_L liquid limit, P_I plasticity index, USCS Unified Soil Classification System, γ unit weight, φ' friction angle, c' effective cohesion, CaCO₃ carbonate content, K_s saturated hydraulic conductivity, US upper soil layers, LS lower soil layers, CAL calcic soil layer, WB weathered bedrock, CL clay of low plasticity, SM silty sand

from the pedological point of view: Ap (0–0.21 m), Bss (0.21–0.68 m) and Bck (0.7–0.9 m).

Below the US level, at depths between 0.9 and 1.5 m, there is a calcic soil layer (CAL), which corresponds to a Ck1 horizon from the pedological point of view. It is characterised by similar texture and plasticity with respect to the upper one, but it has a higher unit weight (20.3 kN/m^3) and higher carbonate content (26.7%) than US level. In the CAL layer, carbonate concretions are significantly dense and their size ranges between centimetre to decimetre. Between 1.5 and 2.0 m, a further layer (C2 horizon from the pedological point of view) has the same textural and plasticity of CAL, but with lower unit weight (19.3 kN/m^3) and a nil content in carbonates. This level can be identified as a clay shale layer (CS), due to its soft and highly plastic consistency, and extends down to the weathered bedrock, at a depth of 3.5–4.0 m from ground level.

The soil layers at Costa Cavalieri test site can be distinguished also on the basis of their shear strength parameters, obtained through direct shear tests. US and CS are characterised by similar values of soil friction angle, equal to 10° and 12° , respectively, instead the CAL layer has a higher friction angle, equal to 18° . All soil layers are characterised by a nil effective cohesion. Oedometric tests, performed on undisturbed samples, revealed how all soil layers are over-consolidated.

Field measurements of saturated hydraulic conductivity, carried out using an amoozometer, showed how it decreases as depth increases. US has the highest value, in the order of 10^{-5} m/s , while CAL and CS are characterised by a saturated hydraulic conductivity of 10^{-7} m/s and 10^{-8} m/s , respectively.

Table 2 summarises the main soil features at Costa Cavalieri test site.

As regards the hydraulic conductivity, it is worth noting that the adopted field measurement technique is sensitive to large scale porosity, such as macropores and fissures. Indeed, experimental evidence shows that the large scale porosity decreases with depth and this is the main reason why both profiles show decreasing hydraulic conductivity with depth.

Moreover, the effect of soil structure on the hydraulic conductivity is demonstrated by the fact that the reduction is larger at Costa Cavalieri test site, where the clay fraction is higher.

Monitoring stations

At both test sites, which were assumed representative of the surrounding area, a hydrological monitoring station was installed. The location was selected due to the presence of past shallow landslides close to the monitoring point and to the typical geomorphological and geological features of the test site. Specific information about the field equipment is reported in Table 3. At both stations, data are recorded with a time frequency of 10 min.

At Montuè test site, the monitoring was installed in March 2012. It integrates meteorological and hydrological sensors (Fig. 3a). The meteorological sensors measure rainfall, air temperature, air humidity, atmospheric pressure, wind speed and direction, and net solar radiation. Hydrological sensors include six time-domain reflectometer (TDR) probes, installed at different depths, three Jet-fill tensiometers and three heat dissipation (HD) sensors, installed in pairs at three different depths, based on the characteristics of the soil layers. Jet-fill tensiometers and HD sensors are in pairs because the former measures the soil water potential for values higher than -10 J/kg (less negative values, lower absolute values), and the latter allows us to obtain soil water potential measurements lower than -10 J/kg (more negative values, higher absolute values). The HD sensor is based on the Flint et al. (2002) equation to convert the measured change in soil temperature after a constant heating period (Bittelli et al. 2012). All field data are collected by a datalogger powered by a photovoltaic panel. A more detailed description of the monitoring station and the probes is reported in Bordoni et al. (2015).

The Costa Cavalieri station was installed in December 2015 (Fig. 3b). The hydrological sensors include five GS3 probes installed at different depths, three MPS-6dielectric sensors, and three T4e-UMS tensiometers, installed in pairs

Table 2 Main properties of soils at various levels at Costa Cavalieri test site

Soil level	Depth m	Gravel %	Sand %	Silt %	Clay %	w_L %	P_I %	USCS class	γ kN/m^3	ϕ' $^\circ$	c' kPa	CaCO_3 %	K_s m/s
US	0.2	1.0	2.3	42.2	54.5	69.2	49.3	CH	19.0	10	0.0	9.8	10^{-5}
	0.4	0.6	2.2	39.7	57.5	71.3	53.1	CH	18.7			9.8	
	0.9	0.5	2.3	45.7	51.5	73.9	53.6	CH	18.6			13.7	
CAL	1.2	2.5	3.2	46.8	47.5	65.5	45.6	CH	20.3	18	0.0	26.7	10^{-7}
CS	1.7	0.1	0.7	42.2	57.0	73.4	51.1	CH	19.3	12	0.0	0.0	10^{-8}

w_L liquid limit, P_I plasticity index, USCS Unified Soil Classification System, γ unit weight, ϕ' friction angle, c' effective cohesion, CaCO_3 carbonate content, K_s saturated hydraulic conductivity, US upper soil layers, CAL calcic soil layer, CS clay shales layer, CH clay of high plasticity

Table 3 Field equipment at the two test sites

	Device	Model	Depth (m)	Accuracy	Range of measure
Montuè					
Soil water content, soil temperature, soil water electrical conductivity	TDR probes	CS610, Campbell Sci. Inc., Logan, UT	0.2, 0.4, 0.6, 1.0, 1.2, 1.4	0.01–0.02 m ³ /m ³	0–1 m ³ /m ³
Soil water potential (< –10 J/kg)	Heat dissipation (HD) sensors	HD229, Campbell Sci., Logan, UT	0.2, 0.6, 1.2	1.5–2.0 J/kg	–10,000/–10 J/kg
Soil water potential (> –10 J/kg)	Tensiometer	Jet-Fill 2725, Soilmoisture Equipment Corp., Santa Barbara, CA	0.2, 0.6, 1.2	1.5–2.0 J/kg	–80/15 J/kg
Rainfall	Rain gauge	52,203, Young Comp., Traverse City, MI	-	0.01 mm	0 mm
Air temperature, air humidity	Thermohygrometer	HMP155A, Campbell Sci. Inc., Logan, UT	-	0.2 °C, 1%	–80/60° C, 0–100%
Atmospheric pressure	Barometer	CS100, Campbell Sci. Inc., Logan, UT	-	0.1 hPa	600–1100 hPa
Wind speed, wind direction	Anemometer	WINDSONIC, Campbell Sci. Inc., Logan, UT-	-	0.01 m/s, 3°	0–60 m/s, 0–359°
Net solar radiation	Net radiometer	NR-LITE 2, Kipp & Zonen, Delft, Netherlands	-	3 W/m ²	-
Datalogger: No. 1 CR1000X (Campbell Scientific, Inc.)					
Costa Cavalieri					
Soil water content, soil temperature, soil water electrical conductivity	GS3 soil moisture sensors	Decagon Devices Inc., Pullman, WA	0.2, 0.4, 0.6, 0.9, 1.7	0.01 m ³ /m ³	0.05–1 m ³ /m ³
Soil water potential (< –10 J/kg)	Dielectric sensors	MPS-6, Decagon Devices Inc., Pullman, WA	0.4, 0.6, 0.9	3 J/kg	–10,000/–9 J/kg
Soil water potential (> –10 J/kg)	Tensiometer	T4e, UMS, Munich, Germany	0.4, 0.6, 0.9	0.5 J/kg	–85/10 J/kg
Meteorological data	Meteorological station of ARPA Lombardia at Fortunago				
Dataloggers: No. 1 DL6 (Delta-T Devices, Cambridge, UK) and No. 2 EM50 (Decagon Devices Inc., Pullman, WA)					

at three different depths, according to the characteristics of soil layers (details are reported in Table 3). Tensiometer data is collected by a DL6 datalogger, and data of water content and from dielectric sensors are collected by two EM50 dataloggers. Meteorological data (rainfall amount, air temperature, air humidity, wind speed and direction) related to the Costa Cavalieri test site are acquired by the meteorological station of ARPA Lombardia at Fortunago, which is located at 501 m a.s.l., 2 km away from the test site.

As for the soil water potential measured at both sites, it is worth noting that this term identifies the potential energy of water in soil, whose units are joules per kilogram (J/kg)

instead of ‘pore-water pressure’ or ‘matric suction’, whose unit is Pa. In fact, the mass basis potential is more clearly related to the concept of energy status of water in soil and it has been preferred over the pressure unit (Campbell and van Schilfhaarde 1981). The authors are aware that this name is not common in the fields of geotechnical and geological engineering, where pressure unit (kPa) is generally preferred, especially when we refer to pore water pressure or matric suction. Nevertheless, if one considers that 1 J/kg is 1 kPa (assuming the density of water equal to 1 Mg/m³), the readability of the following sections should not be compromised.

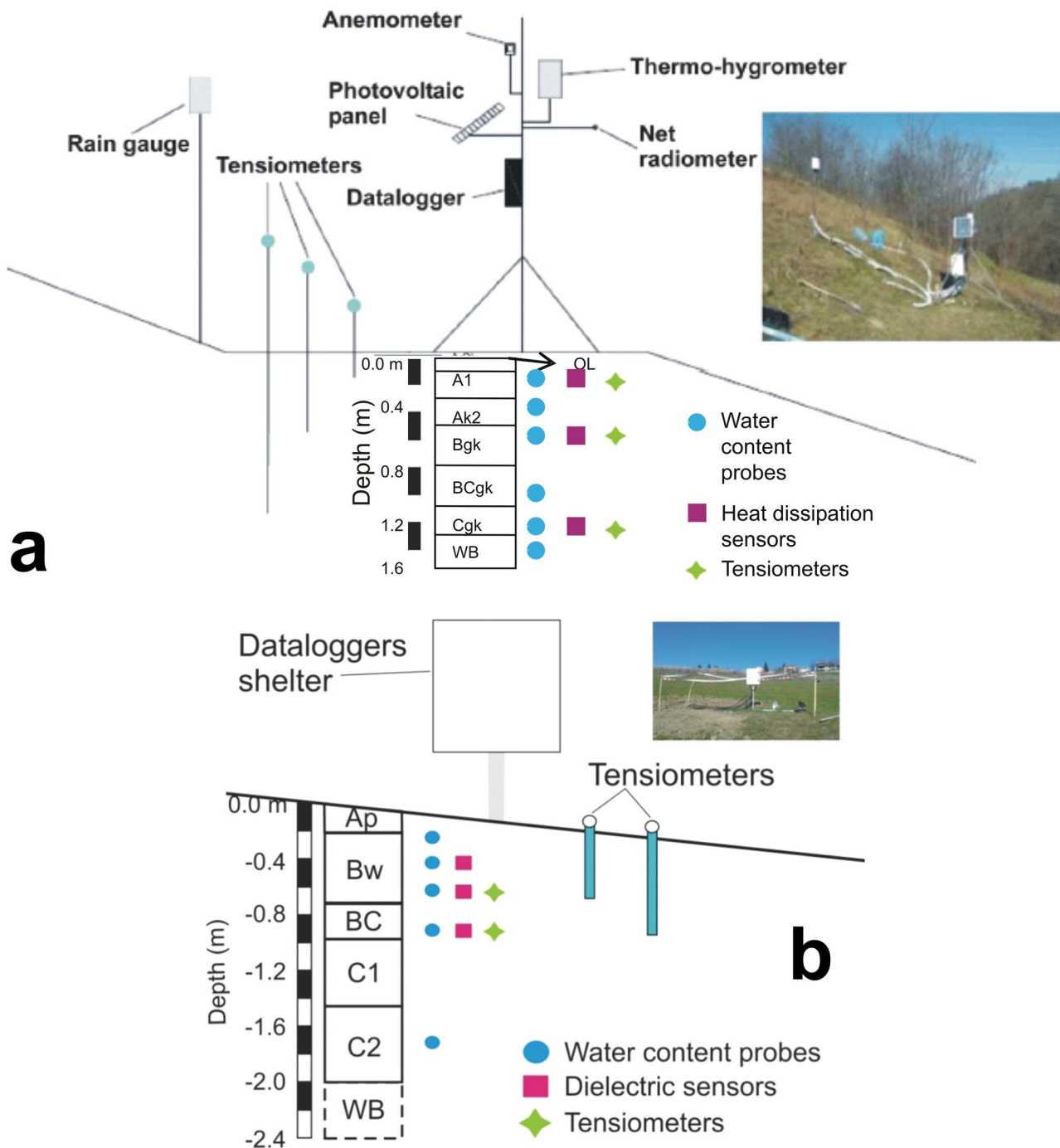


Fig. 3 Schematic representation of the monitoring stations. **a** Montuè. **b** Costa Cavalieri

Installation of field devices

At each monitoring test site, the installation depths of the sensors were chosen according to the representative soil stratigraphy, in order to evaluate in the most appropriate way the soil response along the unsaturated vertical profile, in terms of water content and soil water potential, in relation to different meteorological conditions. In particular, the purpose was

to monitor the hydrological response of the main soil layers at both the test sites, according to the different seasonal and meteorological conditions (Fig. 4).

At both test sites, the monitoring devices were positioned in undisturbed soil layers next to a trench pit, which was purposely dug to allow installation, and were connected to the datalogging system. Both water content and soil water potential sensors were hand-studded in the soil on the uphill

trench pit wall at depths specified in Table 3, and the data logging system was installed on natural undisturbed ground just beside. In this way, underground water flows have been kept in natural conditions and the presence of preferential flows could be assumed negligible. At Montuè station, the meteorological sensors were installed together with the data logging system, except for the rain gauge, which was positioned on the ground next to the trench pit.

The main instrumentation maintenance concerns the distilled water refilling of tubes and caps of the tensiometers, in particular during prolonged dry periods with strong evaporation. After this refilling, air bubbles, which could

be entrapped in the tube during this operation, have to be expelled by pushing a button on the cap. Recovery of the device is in the order of 1–2 h. Furthermore, tensiometers are covered with plastic panels to avoid the water freezing in the caps, especially during winter.

Moreover, values of soil water potential acquired by Jet-fill tensiometers required a correction due to the water column in the device. The correction implied to account for an increase of 1 J/kg (equal to a pressure of 1 kPa) per each 0.1 m of depth in the soil. Thanks to the same water column, it was possible measuring also positive values of the soil water potential (Zhan et al. 2006).

At both test sites, average hourly values of measurements were considered to analyse the soil hydrological trends. For Montuè test site, the time span between 27 March 2012 and 6 June 2019 (about 87 months) was considered, while the monitoring period at Costa Cavalieri test site was between 10 December 2015 and 6 June 2019 (about 42 months).

At Montuè test site, at 0.2 m from the slope surface, soil water potential in the range between 0 and -10 J/kg (corresponding to a pressure range between 0 and -10 kPa) was not measured since November 2012, due to the breakage of the tensiometer installed. Moreover, at Montuè station, no data were acquired in short periods when an incorrect functioning of the station power system occurred. This was linked to periods of prolonged absence of solar light able to recharge the alimentation system through the solar panel. Due to this inconvenience, the station did not acquire data for less than 3% of the total number of days during the 87 months of monitoring.

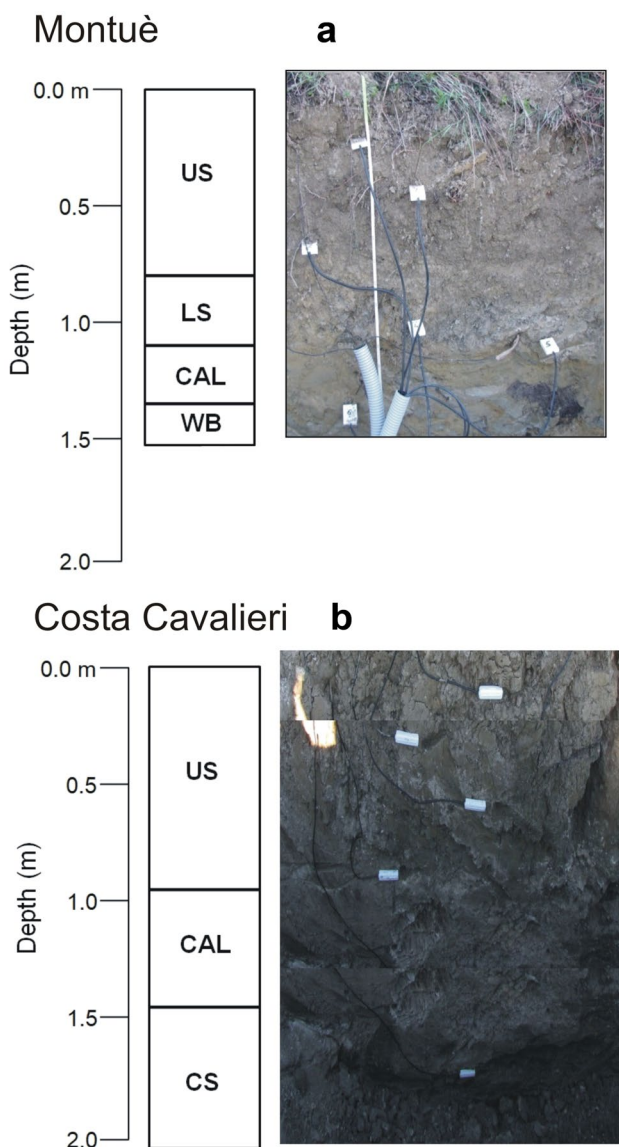


Fig. 4 Installation of the water content probes in the two test sites. **a** Montuè. **b** Costa Cavalieri. Sensors have been installed in each of the different soil layers present in the representative stratigraphic profile of each test site

Results and discussions

Meteorological data

Before analysing the main hydrological trends in correspondence of the two monitored test sites, it is important to evaluate the main meteorological and climatic features of the studied slopes, which could have effects on the soil behaviour.

For this aim, complete yearly trends of most significant meteorological parameters acquired for the two test-slopes were analysed.

Figure 5a shows daily rainfalls and daily mean air temperature at Montuè sample site between 1 January 2013 and 31 December 2018. It is evident how the climate regime is characterised by the alternation of a hot season, from April to October (globally identified as ‘summer’ in this paper), and a cold season, from November to March (globally called ‘winter’ herein). Rainfalls are well distributed during the year but are more abundant in intermediate seasons, i.e.,

March–April and October–November. The maximum daily rainfall peak of 67.2 mm was attained in October 2014, and two further peaks of 60 mm each were attained in March and October 2014. On the 6-year time-span, the mean annual rainfall amount was 604.5 mm, with a maximum of 993.4 mm in 2014 and the minimum of 324.6 mm in 2017.

Figure 5b shows the solar radiation. The trend confirms that this site is characterised by higher solar radiation during summer and much less solar radiation in winter. Moreover, it has been possible to calculate a mean annual level of solar radiation equal to $24 \cdot 10^3 \text{ W/m}^2$, with a maximum of $26.3 \cdot 10^3 \text{ W/m}^2$ in 2014 and a minimum of $22.6 \cdot 10^3 \text{ W/m}^2$ in 2017.

Figure 6 shows daily rainfalls and daily mean air temperature at Costa Cavalieri test site between 1 January 2016 and 31 December 2018. It is evident how also in this case the climate is characterised by the alternation between the hot season (from April to October) and the cold one (from November to March). As in Montuè test site, rainfalls are well distributed during the year but are more abundant in

intermediate seasons, March–April and October–November. Climatic data acquired on a time span of three years seem to show that in the last year rainfalls were less intense but more frequent with respect to the previous 2 years.

A comparison of the typical climatic conditions between the two test sites was also performed. Figure 7 reports the mean monthly air temperature and the cumulated monthly rain for the two sample sites. These data are reported for both sites only for 2016, 2017 and 2018, since in the previous 3 years, only the monitoring station at Montuè was activated. Air temperature is slightly different between the two test sites. Costa Cavalieri test site was averagely 1°C colder than Montuè. The reason is probably related to the difference in elevation, since Montuè is located at 185 m a.s.l., instead the ARPA station at Fortunago (near to Costa Cavalieri) is at 501 m a.s.l.. The mean difference in monthly cumulated rainfall was 17 mm only, even if the difference reached 60 mm in some months of the considered time span. It is worth noting that the two sites are characterised by different rainfall amounts. In particular, rainfalls occurred in the

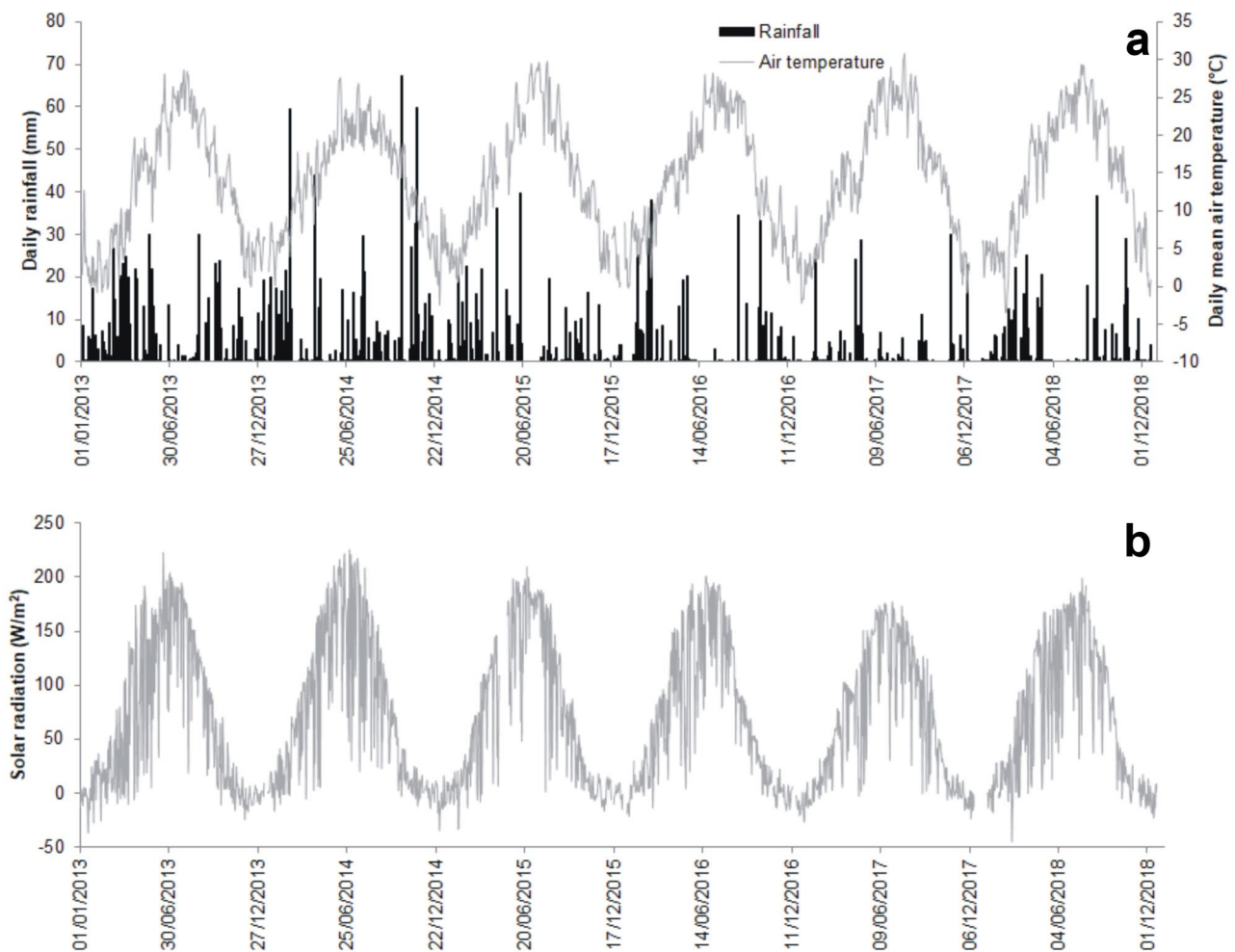


Fig. 5 **a** Daily rainfalls and daily mean air temperature at Montuè test site. **b** Daily solar radiation at Montuè test site (dates: dd/mm/yyyy)

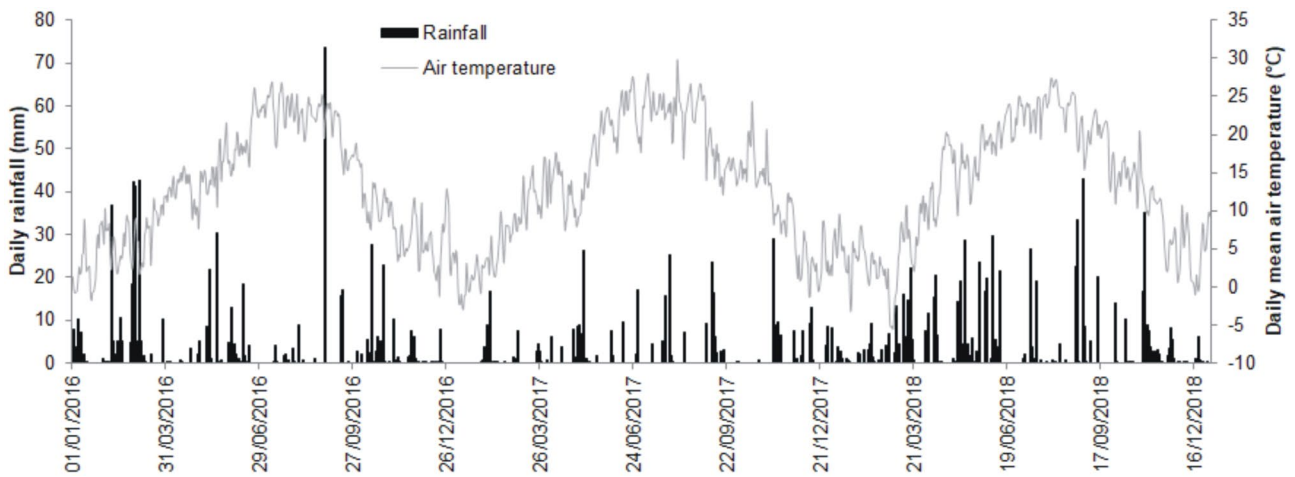


Fig. 6 Daily rainfalls and daily mean air temperature at Costa Cavalieri test site (dates: dd/mm/yyyy)

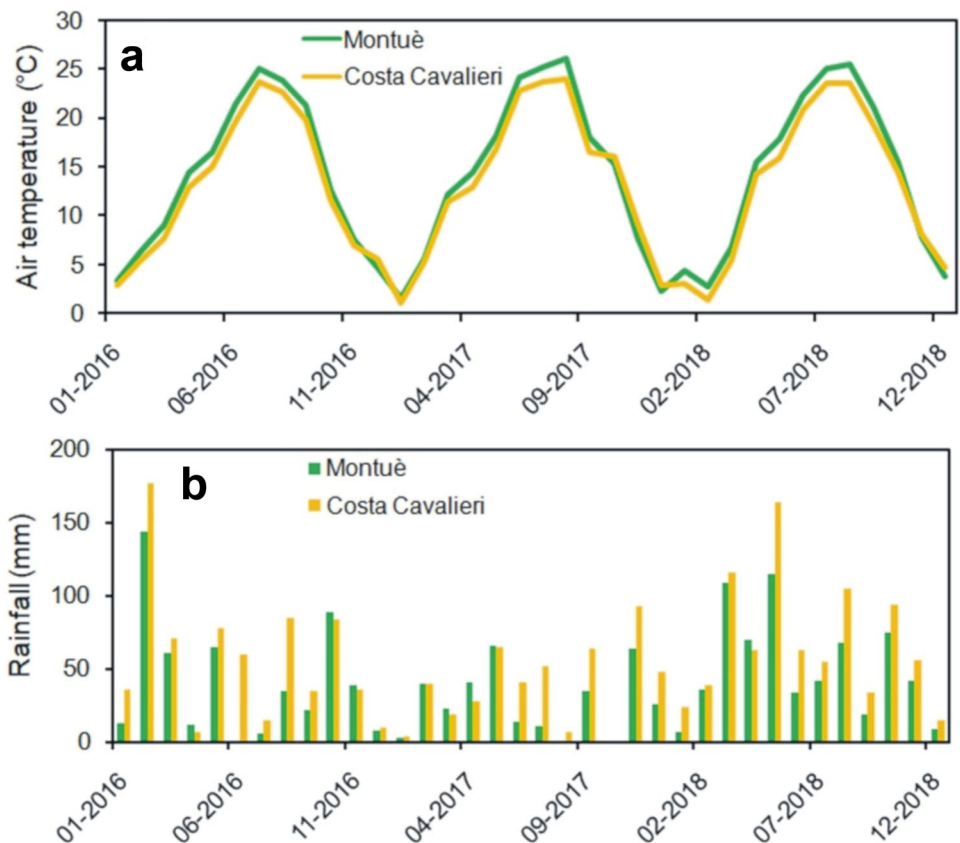
last three years at Costa Cavalieri appear always higher with respect to those occurred at Montuè, although the two sites are distant only 18 km from each other. This variation could be related to the peculiar orography of the two areas. Moreover, this difference over a small area reflects the importance of acquiring meteorological data on a small geographic grid, and of installing a specific weather station at each study site. Relying on existing networks of meteorological stations may

not provide appropriate data, at least for site-specific problems and detailed phenomena.

Soil temperature

Figure 8 shows the trend of soil temperature measured at three different depths (0.2, 0.6 and 1.2 m below the ground

Fig. 7 Monthly average air temperature **a** and cumulated rainfall **b** recorded at Montuè and at Costa Cavalieri sites in the period 2016–2018



surface) at Montuè test site and at five different depths (0.2, 0.4, 0.6, 0.9 and 1.7 m below the ground surface) at Costa Cavalieri test site. It is evident how soil temperature obviously follows the trend of air temperature at both sites and at different depths, except in the CS layer at 1.7 m below ground at Costa Cavalieri test site (Figs. 5a and 6). As a consequence, in the first 1.0–1.2 m below ground level, higher soil temperatures were reached during hot months, from April to October, with peaks of 26–28 °C in the shallowest monitored horizons (US at 0.2 m from ground level). In both sites, it is worth observing that the highest temperatures have been registered in the soil during the hot season in 2017. As it will be explained in the following, these higher temperatures correspond to smaller values of soil water content and higher values of soil water potential with respect to similar seasons in other years. The lowest temperatures were reached during cold months, especially during winter season from December to February. In these periods, soil temperatures in the first 1.0–1.2 m below ground level decreased to values lower than 8 °C, with values of 3–4 °C in the US layer at 0.2 m from ground during the coldest periods at both test sites.

It is also clear how the range between maximum and minimum temperature is reduced as the depth increases. This is particularly evident in the CS layer (1.7 m from ground level) at Costa Cavalieri test site (Fig. 8b). This layer is less influenced by the seasonal changes of air temperature, which instead affects the shallowest soil layers. Moreover, the highest and the lowest values of soil temperatures typical of this horizon (18–19 °C and 10–11 °C, respectively) are recorded slightly shifted with respect to the ones measured in the shallowest soil layers. This shift, which is of about 15–20 days,

is due to the time required for heat diffusion from the ground surface down to this depth.

Volumetric water content and soil water potential

Figures 9 and 10 show the water content and soil water potential trends at Montuè and Costa Cavalieri test sites, respectively.

In the first 3 months after the installation of the monitoring stations, both water content and soil water potential showed a relatively high degree of scattering (Figs. 9 and 10). Sensors required a rather long period to reach equilibrium. In fact, the ceramic stone of some probes (tensiometers, HD and dielectric sensors) and the sticks of the water content probes required a certain time to progressively adhere to the surrounding soil after installation, in order to allow suitable data acquisition. As a consequence, reliable trends of the hydrological parameters could be acquired from June 2012 and from February 2016 at Montuè and at Costa Cavalieri, respectively.

In order to verify the level of confidence of field soil water potential measurements, some laboratory tests were carried out by using the filter paper on samples collected in different seasons, and field tests were performed through a portable tensiometer (Model Quick Draw, Soilmoisture Equipment Corp.) (Table 4). They gave soil water potential values very similar to those measured by the field monitoring systems. The differences were in the order of 1–2 J/kg when the soil was very close to saturation, and 10–20 J/kg when it was far from the saturated conditions. Also, field water content measurements had a good level of confidence, with differences lower than 0.05 m³/m³ between field and laboratory values, from samples collected close to the monitoring points during different seasons at different depths

Fig. 8 Soil temperature trends at the two test sites. **a** Montuè. **b** Costa Cavalieri

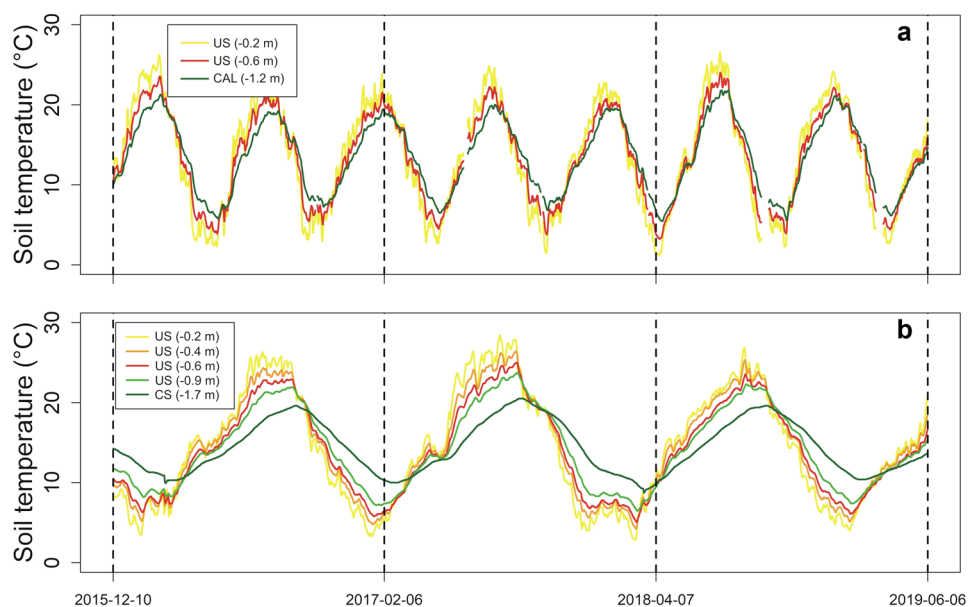
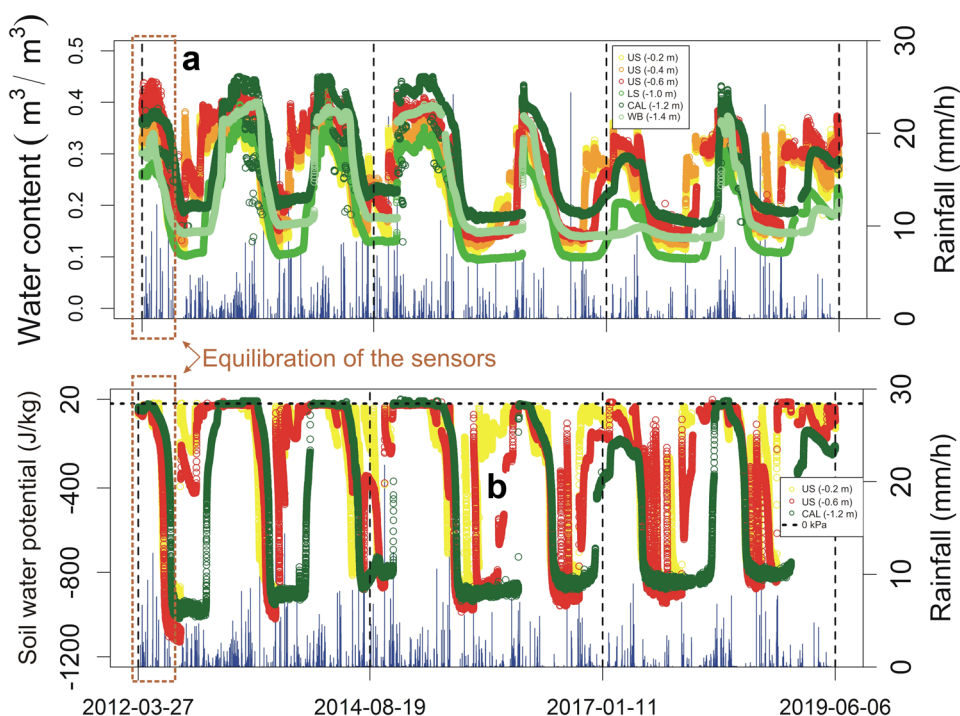


Fig. 9 Water content **a** and soil water potential **b** measured at different depths at Montuè test site for the whole monitoring period



(Table 4). Thanks to these indications, field data allowed for identifying the main hydrological features of the test site slope.

From Figs. 9 and 10, it could be observed that, at both test sites, water content and soil water potential dynamics are strictly connected to dry and rainy periods. Different hydrological behaviours can be identified in the soil profiles.

During hot periods, characterised by a lower amount of rainfall, decreases of water content and of soil water potential are much faster at Montuè than Costa Cavalieri (Figs. 9 and 10). In all the investigated levels at Montuè test site, in less than 1 month without significant cumulated rainfall, water content and soil water potential came back to the values reached before the previous re-wetting. At Costa

Fig. 10 Water content **a** and soil water potential **b** measured at different depths at Costa Cavalieri test site for the whole monitoring period

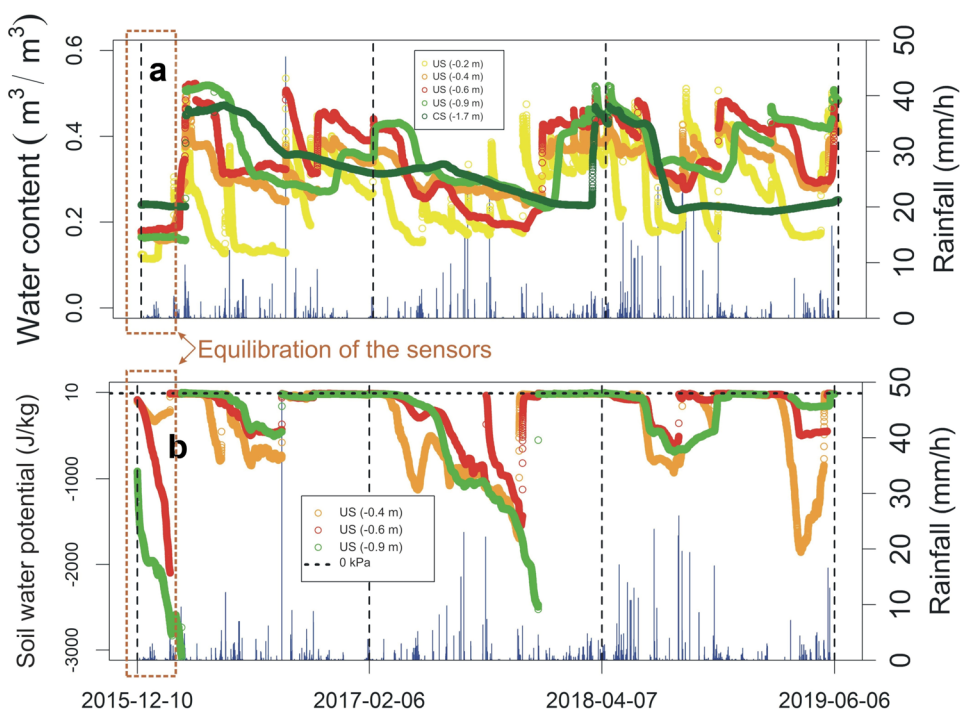


Table 4 Comparison between laboratory measured and field monitored data of soil water content and soil water potential

Laboratory test or device	Test site	Depth (m)	Soil water potential (J/kg)- laboratory	Soil water potential (J/ kg)-field monitoring
Filter paper	Costa Cavalieri	0.2	-7.0	-8.9
Filter paper	Montuè	0.2	-200.0	-201.9
Filter paper	Montuè	0.6	-15.0	-10.8
Filter paper	Costa Cavalieri	0.6	-200.0	-219.3
Filter paper	Montuè	1.2	-10.0	-9.6
Portable tensiometer	Montuè	0.2	-7.1	-9.6
Portable tensiometer	Montuè	0.6	-10.4	-11.2
Laboratory test or device		Depth (m)	Soil water content (m ³ /m ³)- laboratory	Soil water potential (m ³ /m ³)-field monitor- ing
Direct heating	Costa Cavalieri	0.2	0.19	0.14
Direct heating	Montuè	0.2	0.33	0.32
Direct heating	Montuè	0.6	0.13	0.14
Direct heating	Costa Cavalieri	0.6	0.37	0.34
Direct heating	Montuè	1.2	0.44	0.42

Cavalieri, in the same month, only the shallowest soil level (US at 0.2 and 0.4 m from ground), came back to the driest soil conditions, while the deeper layers (US below 0.4 m from ground level, CAL and CS) needed about 40–60 days to reach the driest soil condition. This difference is related to different hydraulic conductivity of the materials forming the two soil profiles, where Montuè soils are one order more permeable than those at Costa Cavalieri, except for similar values in the shallowest levels. Besides the difference in soil texture (and thus in hydraulic conductivity), the two sites have a great difference in vegetation (one is wild, the other is cultivated). The presence of roots and root channels and the seasonal water uptake by roots surely affect the observed response after precipitation periods, but this aspect is beyond the scope of the present work and has not been considered herein.

In both sites, US layers down to 0.6 m from the ground level had quicker response than deeper layers, as consequence of rainfalls occurred in winter and spring months, following a prolonged dry period. A daily rainfall of 25–35 mm was enough for increasing water content of more than 0.2 m³/m³ and soil water potential of more than 100 J/kg in the most superficial layers (Figs. 9 and 10). This fast increase is more evident in correspondence of thunderstorms with at least 20 mm of cumulated rain in 4–5 h. During these storms, soil water potential increase due to re-wetting is not coupled with a correspondent increase in water content (Figs. 9 and 10). This behaviour could be linked to non-equilibrium processes due to a fast infiltration phase in which soil water potential or water content trend lags behind each other by the water retention equilibrium, as previously observed by other authors (Rogers and Klute 1971; Ross and Smettem 2000;

Simunek et al. 2003; Vogel et al. 2010; Diamantopoulos et al. 2012). At Costa Cavalieri test site, desiccation cracks and other macro-voids, which arise during dry periods for shrinking processes of the silty clay soils, could increase this rapid re-wetting through a fast rainwater infiltration (Fig. 11), as will be explained in detail in the following.

During the analysed time spans, re-wetting of the soil horizons below 0.6 m from ground was as fast as for the shallowest levels, even if it occurred in correspondence with more intense events characterised by at least 70 mm of rain fallen in 50 h (Figs. 9 and 10).

At both sites, during the coldest period of the year, which generally corresponds to the winter and spring months between December and May, soil approaches saturated conditions all along the profile, as testified by the highest values of soil water content (0.45 m³/m³ at Montuè and 0.52 m³/m³ at Costa Cavalieri) and by soil water potential near 0 J/kg (Figs. 9 and 10). The higher the amount of rainwater fallen during the cold season, the longer are these periods. Considering a monitoring period common to both test sites, soil water potential values in the different soil layers kept higher than -10 J/kg only during 20–35 days between December and May 2016, 2017 and 2019, characterised by a limited amount of rain fallen in the cold months (averagely 241 mm and 251 mm of cumulated rain between December and May at Montuè and Costa Cavalieri, respectively). Instead, between December and May 2018, soil water potential values in the different soil layers of the two test sites kept higher than -10 J/kg for 138 days, as a consequence of a more rainy period (337 mm and 406 mm of cumulated rain between December and May at Montuè and Costa Cavalieri, respectively) than in other years.

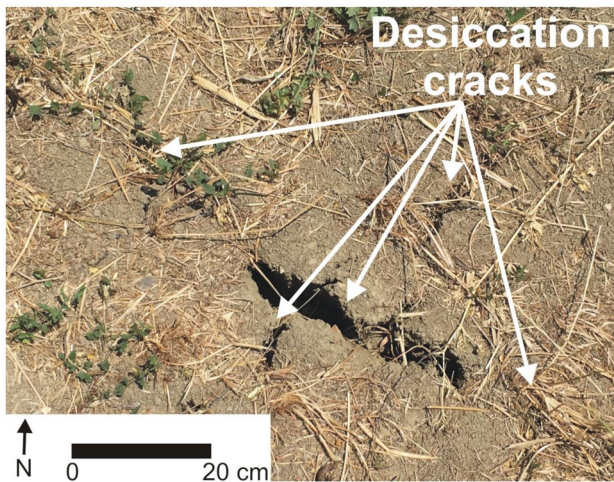


Fig. 11 Desiccation cracks forming in superficial layers of Costa Cavalieri monitored slope during prolonged dry periods

In similar hydrological conditions, the CAL layer at Montuè soil profile could reach complete saturation (Fig. 9), as testified by the values of soil water potential, which kept quite steady around 0 J/kg during spring 2018 as well as during winter and spring months in 2013, 2014 and 2015 (Bordoni et al. 2015). Due to the low permeability of the weathered bedrock below this layer, the infiltrated rainwater tends to stagnate in the CAL layer and forms a transient perched water table. Soil water potential in this layer can further increase up to positive values around 1–3 J/kg after intense rainfall events, characterised by a duration of at least 20 h and a cumulated amount of at least 25 mm. Even if there are no field measurements of hydrological parameters between 0.9 and 1.5 m, a similar condition could be found also at Costa Cavalieri site, where the CAL layer has similar geotechnical and physical features to the corresponding CAL level at Montuè and is also limited below by a less permeable layer (CS level). Moreover, it is worth noting that the water content measured in the soil below the CAL layer is lower than the overlying CAL layer at both test sites, confirming the contrast of permeability which limits the infiltration of rainwater below the CAL layer.

The increase of soil water potential up to positive values testifies to an uprising of the perched water table into overlying layers (Li et al. 2013). In particular, this uprising was observed in two monitored events which caused the triggering of shallow landslides in these test site slopes or in the surrounding areas. At Montuè test site slope, during 28 February–2 March 2014 event (68.9 mm of rain in 42 h), US layers down to 0.7 m and the deeper CAL horizon behaved as during other rainfall events in winter–spring months and in other wet periods. On the contrary, intermediate LS level at 1.0 m, which is positioned between US and CAL layers, was affected by a significant increase of the water content.

This increase testified the uprising of a perched water table, which is usually present in the CAL layer during wet periods, up to 1.0 m, leading the LS horizon to become completely saturated. In the same way, at Costa Cavalieri test site, during the rainfall event that occurred on 5–6 March 2016 (42.6 mm of rain in 24 h), US layer down to 0.6 m from the ground level behaved as during other rainfall events in winter–spring months and in other wet periods. By contrast, US level at 0.9 m was affected by a significant increase in soil water potential towards positive values, passing from 0 to 7 J/kg. This increase testified the uprising of a perched water table, normally located in the CAL layer during wet periods, up to 0.9 m, similarly to the mechanism observed at Montuè site.

This hydrological behaviour of a perched water table uprising can be considered the triggering mechanism of rainfall-induced shallow landslides in the test site slopes, as already noticed in previous works in other geomorphological and environmental contexts (Tohari et al. 2007; Li et al. 2013; Lu and Godt 2013; Tang et al. 2015). It is worth noting that this triggering mechanism is only one of the possible conditions which could induce shallow slope instabilities during rainfall events. In fact, shallow landslides can be triggered also as consequence of downward rainwater wetting front till layers with low shear strength properties during intense and concentrated thunderstorms or due to breakthrough infiltration of rainwater along fractures and holes in the soil. These two last triggering mechanisms are very common in landslides occurring in loess (Tang et al. 2015) and have also been described by Shao et al. (2015) for other kinds of soils.

At both test sites, as a consequence of rainy events that occurred during cold/wet periods, the infiltrated rainwater reached the US layers down to 0.6 m from the ground in about 12–15 h, which is faster than the arrival time during autumn re-wetting events, due to the higher initial soil water content (Figs. 9 and 10). The similar arrival time is related to the similar hydraulic conductivity of US layers at both sites (10^{-5} m/s). Moreover, during these events, the wetting front is also able to reach deeper levels in the soil profile. In particular, at Montuè site, it reaches the LS layer at 1.0 m in almost 18–20 h and the CAL layer at 1.2 m almost 25 h (Fig. 9). Instead, at Costa Cavalieri test site, the wetting front takes about 16–18 h to reach the US level at 0.9 m of depth (Fig. 10). This shorter arrival time is related to the higher conductivity of soils between 0.6 and 1.0 m of depth at Costa Cavalieri site than the ones at Montuè (10^{-5} m/s at Costa Cavalieri, 10^{-6} m/s at Montuè).

It is also important to highlight that the CS layer at 1.7 m in Costa Cavalieri test site shows a very smoothed trend in terms of water content (Fig. 10) and is affected only by prolonged periods of intense rainfalls or significant evaporation due to its depth in the soil profile.

Relationship between water content and soil water potential on a small time span

To analyse the soil behaviour during ordinary rainfalls occurring both in hot (summer) and cold (winter) seasons, it appears useful to represent the relationship between soil–water content and soil water potential at each observation depth, for the two test sites, on time spans shorter than one season. In the following sections, for each sample site and for each depth, different wetting and drying phases based on experimental measurements will be shown. Only one diagram that could be assumed as representative for each season has been selected. The observed wetting–drying cycles are compared with SWCCs. In particular, as regards the Montuè test site, reference SWCCs are those obtained by Bordoni et al. (2017) for the same soils. Instead, as regards the Costa Cavalieri test site, SWCCs are only supposed to be the most likely, since the analytical process adopted by Bordoni et al. (2017) has not yet been applied to these soils and will be the subject of a future publication. For Costa Cavalieri soils, we used typical SWCCs for clayey soils (Lu and Godt 2013), setting the saturated water content (θ_s) equal to the highest values of water content measured in field during dry and wet periods.

The Van Genuchten equation fitting parameters of main drying curve (MDC) and main wetting curve (MWC) for the different soil levels, adopted for the SWCCs, are reported in Table 5. Although the frequency of field data acquisition is 10 min, as mentioned above, the values were first aggregated in order to obtain a single daily value. For a better graphic representation of the wetting and drying paths, by following the same process adopted by Papa et al. (2013), some daily data were omitted, after having ascertained that they had a negligible deviation from the mean average trend. Therefore, in the following graphs, only some representative dates are shown.

Montuè test site

Particularly interesting is considering the soil behaviour at three different depths during a relatively dry period, which corresponds to late spring–early autumn. For instance, the period between 8 May and 3 November 2014, which corresponds to summer season, characterised by relatively higher temperatures, has been considered. Figure 12 shows seven alternating drying and wetting phases at a depth of 0.2 m in semi-logarithmic plot (Fig. 12a) and in decimal scale (Fig. 12b) to observe the loops in detail. Figure 12a shows how the trend of repeated drying paths follows the shape of the MDC obtained by Bordoni et al. (2017), although it appears closer to the MWC. Instead, wetting phases, which always follow the occurrence of rainfall events, appear as sudden and drastic reductions in water potential with consequent increase in water content. All the points at the end of wetting paths fall below the MWC. This behaviour is much more evident in Fig. 12b. Starting since 8 May (point 1 in Fig. 12b), the soil undergoes a drying phase until 14 June (point 2), when a daily rainfall of 16.9 mm, followed by further 15.1 mm on 15 June, causes a wetting phase until reaching the minimum soil water potential on 17 June (point 3). Starting from point 3, a prolonged drying phase occurs until 24 July (point 4), when a rainfall of 15.3 mm and a new one of 29.7 mm on 26 July cause a new wetting phase, which ends on 1 August (point 5). Few and slight further rainfall events that occurred in this period do not cause any significant change. A drying phase follows from 1 August (point 5) until 1 October (point 6), when slight rainfalls, followed by an abundant rainfall of 67.2 mm on 13 October, give rise to a further wetting phase until reaching the minimum soil water potential on 18 October (point 7). Although air temperature in this season is rather low, between 18 October (point 7) and 3 November (point 8) soil water potential increases in the range between 28 and 173 J/kg, showing a further drying

Table 5 Van Genuchten equation fitting parameters of main drying curve (MDC) and main wetting curve (MWC) for the different soil levels at Montuè and Costa Cavalieri test sites

	Depth (m)	Drying (MDC)				Wetting (MWC)			
		θ_{sd} (m ³ /m ³)	θ_{rd} (m ³ /m ³)	α_d kPa ⁻¹	n_d -	θ_{sw} (m ³ /m ³)	θ_{rw} (m ³ /m ³)	α_w kPa ⁻¹	n_w -
Montuè									
US	0.2	0.33	0.02	0.003	1.57	0.32	0.02	0.007	1.62
US	0.6	0.4	0.01	0.012	1.38	0.37	0.01	0.017	1.4
CAL	1.2	0.44	0.01	0.013	1.19	0.4	0.01	0.014	1.21
Costa Cavalieri									
US	0.4	0.49	0.01	0.007	1.3	0.41	0.01	0.017	1.4
US	0.6	0.51	0.01	0.017	1.3	0.43	0.01	0.03	1.6
US	0.9	0.51	0.01	0.017	1.3	0.45	0.01	0.03	1.6

MDC main drying curve, MWC main wetting curve, θ_{sd} saturated water content of MDC, θ_{sw} saturated water content of MWC, θ_{rd} residual water content of MDC, θ_{rw} residual water content of MWC, α_d , n_d : fitting parameters of MDC, α_w , n_w : fitting parameters of MWC, US upper soil layers, LS lower soil layers, CAL calcic soil layer, CL clay of low plasticity, SM silty sand

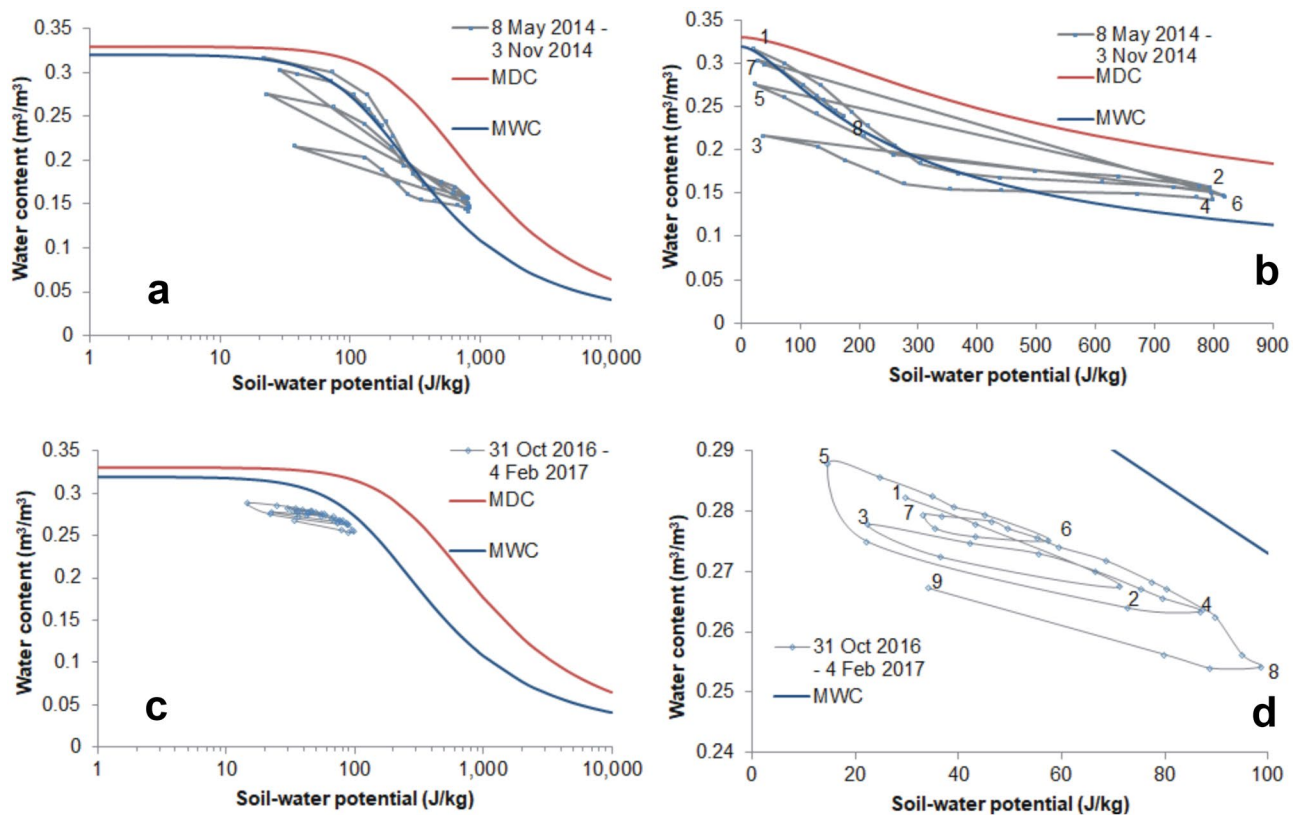


Fig. 12 Montuè test site soil at depth of 0.2 m (US). **a** During summer with data reported in logarithmic scale. **b** During summer with data reported in decimal scale. **c** During winter with data reported in logarithmic scale. **d** During winter with data reported in decimal scale

phase, also affected by evapotranspiration of shrubs that are still present in early autumn. It appears evident how wetting paths are often much faster than drying phases.

Except for this last drying phase, all previous cycles cover a water potential range of about 800 J/kg , while water content ranges between 0.15 and 0.33.

In analogy to what has been shown for the dry and hot period (summer), it is interesting considering also soil behaviour during a relatively wet period (winter). For instance, it is worth considering the period between 31 October 2016 and 4 February 2017, which corresponds to fall and winter season, characterised by relatively lower temperatures. Figure 12c reports data in semi-logarithmic plot together with MDC and MWC obtained by Bordoni et al. (2017) for the soil at 0.2 m of depth. It can be observed how experimental points are all below with respect to the estimated MWC. Figure 12d shows in detail on a decimal scale the alternating drying and wetting phases (from point 1 to point 9), covering soil water potential fluctuations between 17 and 100 J/kg . Wetting paths are always a consequence of rainfall events. It can be noticed how in each cycle the drying path is always higher than the wetting one, i.e., at the same soil water potential value, water content is higher in the drying path with respect to the wetting path. It is consistent with the well-known hysteretic behaviour, although, as

it is shown, different cycles characterise the soil hydraulic behaviour. At 0.2 m in the winter season, hysteretic cycles cover a water potential range of about 100 J/kg , while water content ranges between 0.25 and 0.29.

At greater depth (0.6 m), during the hot period between 15 May and 3 November 2014, the soil undergoes alternative phases of drying and wetting as well (Fig. 13). Figure 13 a shows how the trend of different cycles is very close to the MDC obtained by Bordoni et al. (2017). Even in this case, all drying and wetting phases are directly affected by precipitation. The shape of hysteresis loops can be observed much better if data are reported in decimal scale (Fig. 12b). The first drying phase occurs between 15 May (point 1) and 26 July (point 2) and covers a soil water potential of about 850 J/kg . Rainfalls that occurred in the middle of June do not cause any important change, like in the above soil layer. The subsequent wetting phase that covers a potential range of about 500 J/kg occurs as a consequence of rainfalls of 15.3 mm and 29.7 mm on 24 July and on 26 July, respectively (until reaching point 3 on 2 August). A new drying phase, covering the same potential range of 500 J/kg , starts on 2 August and continues until 1 October (point 4), when slight precipitations, followed by an abundant rainfall of 67.2 mm on 13 October, give rise to a further wetting phase, covering about 800 J/kg (until reaching point 5 on 14

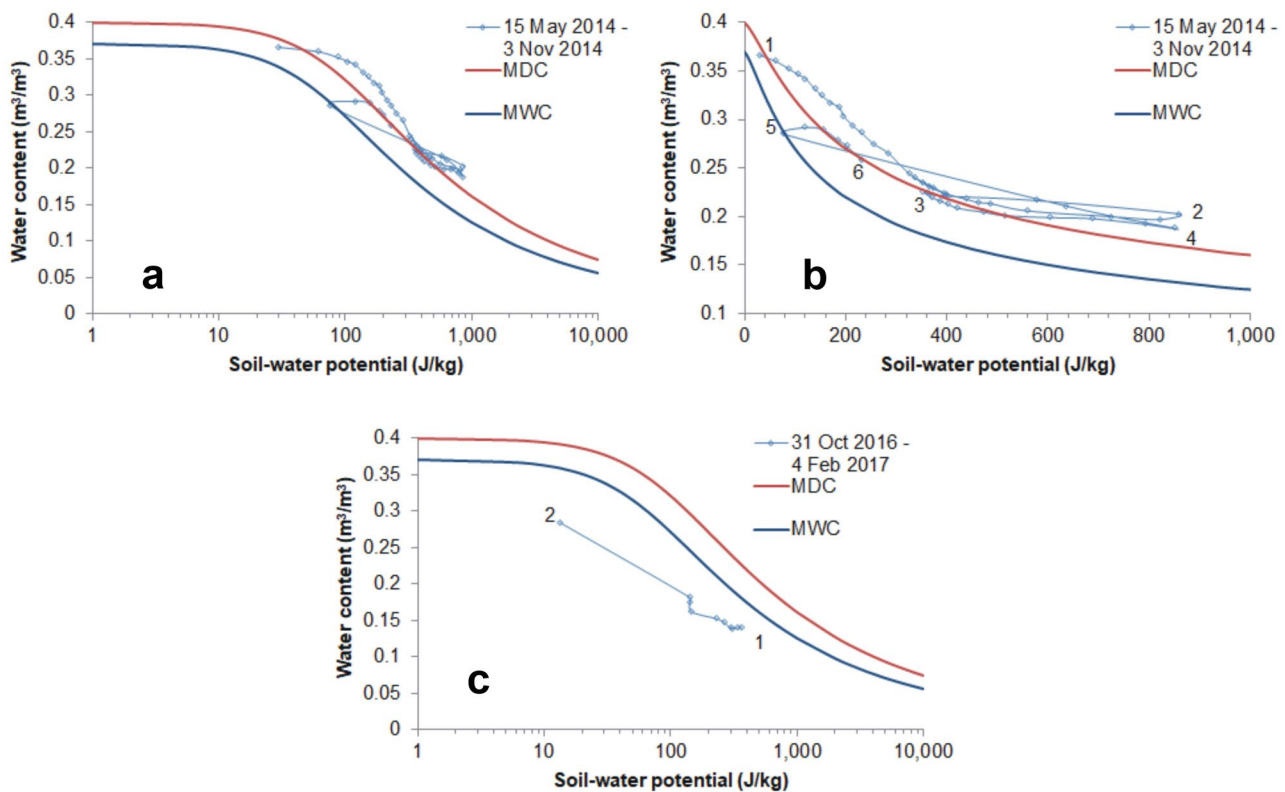


Fig. 13 Montuè test site soil at depth of 0.6 m (US). **a** During summer with data reported in logarithmic scale. **b** During summer with data reported in decimal scale. **c** During winter with data reported in logarithmic scale

October). The last drying phase, lasting from 14 October to 3 November (point 6), confirms the behaviour observed at 0.2 m, although a slight increase of the water content value is within the measurement uncertainty of the TDR probe. However, these loops are consistent with the MDC obtained by Bordoni et al. (2017).

At a depth of 0.6 m, a unique wetting path is observed during winter between 31 October 2016 (point 1) and 4 February 2017 (point 2), covering a soil water potential range of about 350 J/kg (Fig. 13c). Although not shown in Fig. 13c, the wetting phase continues until the end of February. It is evident how, at this depth, intermediate rainfalls do not cause any significant change in the wetting phase, as it was explained above. The wetting path is always below the MWC estimated by Bordoni et al. (2017).

Unlike in the shallowest layers, at a depth of 1.2 m only two phases can be observed in the summer period (Fig. 14a): the first is a drying phase covering a soil water potential range of more than 850 J/kg, which starts on 15 May 2014 (point 1) and continues until 31 July (point 2), when the wetting path begins after the precipitations of 15.3 mm and 29.7 mm occurred on 24 July and 26 July, respectively. In this wetting path, the reduction in soil water potential values

is rather limited at first and the water content remains constant (around point 2). Thereafter, following the abundant precipitations that occurred between 4 and 15 November, soil water potential is reduced by about 400 J/kg and the water content increases from 0.22 to 0.26, reaching point 3 on 15 November 2014. At the same time, since the end of October, a decrease in air temperatures was also recorded. In this case, both drying and wetting phases appear very close to the MWC obtained by Bordoni et al. (2017).

At a depth of 1.2 m, only a wetting phase is observed in winter (Fig. 14b). This is characterised by a decrease in soil water potential from 846 J/kg on 31 October 2016 (point 1) to 330 J/kg on 4 February 2017 (point 2). Even in this case, intermediate rainfalls do not cause any significant change in the wetting phase and the wetting path is below the MWC estimated by Bordoni et al. (2017).

It could be observed that the different behaviour of shallow layers with respect to the deep ones is due to the slower dynamics of soil water redistribution with depth. Shallow layers experience infiltration and redistribution, as a consequence of rainfall events, with fast responses of variation in soil water potential and water content. Therefore, hysteric cycles are usually of shorter duration in the shallow layers with respect to the deep ones. Moreover, the surface layers

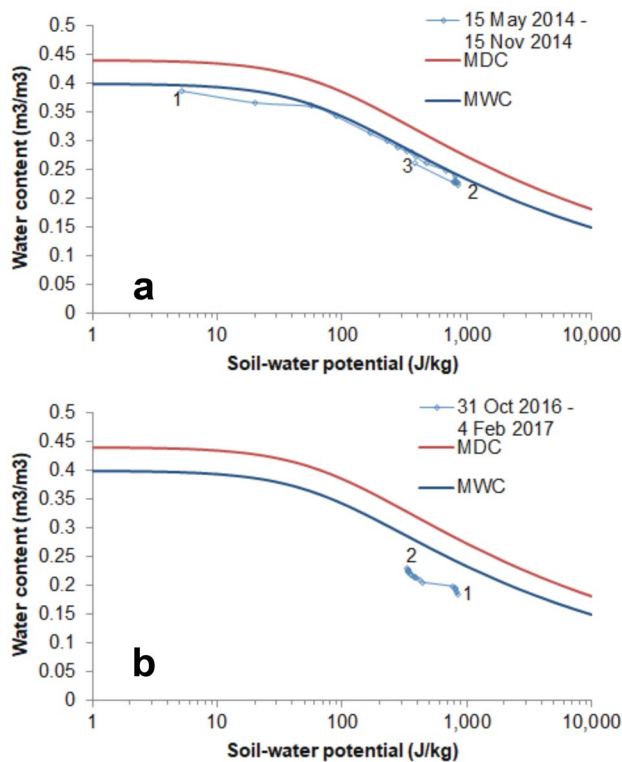


Fig. 14 Montuè test site soil at depth of 1.2 m (CAL) during summer **a** and winter **b**

undergo more intense processes of plant water uptake and evaporation cycles than the deeper ones.

The detailed monitoring in different thin soil sub-layers at the Montuè test site and the comparison with the SWCC model, composed of both MDC and MWC, shows how this model is not fully suitable to reproduce the real soil hydraulic behaviour, not only for each sub-layer but a fortiori for the whole shallow soil layer down to 1.2 m of depth. In other words, the one-hysteretic cycle model seems not to be appropriate, even though the soil is classified as CL from the ground level down to 1.2 m at the Montuè test site. Instead, due to the soil texture and fabric, at Montuè test site the downward water flow appears rather uniform, with very limited preferential pathways, since non-equilibrium conditions have rarely been observed.

Costa Cavalieri test site

Also for the Costa Cavalieri test site, it is useful considering the soil behaviour during a relatively dry period (late spring–early autumn) and during a wet period (autumn–winter). In this case, drying–wetting cycles are compared with SWCCs assumed to be representative due to similarity with other soils of the same characteristics.

The dry period is assumed to be between 1 April and November/December in 2017, which corresponds to the summer–autumn season, with relatively high air temperatures.

At a depth of 0.4 m, during April, May and June 2017, cycles with variations in soil water potential values between 400 and 1600 J/kg and water content between 0.25 and 0.32 are observed (Fig. 15a). These cycles are very close to the MDC.

Figure 1b shows in more detail the nine alternating drying and wetting phases on a decimal scale. The latter are always a consequence of rainfall events. In particular, starting since 1 April (point 1), the soil undergoes a drying phase until 3 May (point 2), when a cumulative rainfall of 22.8 mm in 3 days causes a subsequent wetting phase. The latter lasts until 1 June (point 3), when a new drying phase starts and continues until 2 July (point 4). These three cycles cover a soil water potential range of about 600 J/kg. During July and August 2017, variations in both soil water potential and water content as consequence of rainfall are more limited.

Figure 15b also shows the sequence from point 4 to point 9, which can be interpreted as ‘short’ drying and wetting cycles. Finally, since 31 August 2017 (point 9), the drying process begins, which continues up to a soil water potential of 1600 J/kg until 4 November (point 10), when a rainfall of more than 20 mm causes a decrease in soil water potential (not shown in the figure). Rainfall that occurred in September 2017 does not cause significant variations, while in October no rainfall occurs. It is worth noting that in each cycle the drying path is always higher than the wetting one and this is consistent with the typical hysteretic behaviour. Figure 15c shows the soil behaviour at the same depth of 0.4 m. On 4 November 2017 the soil water potential is rather high (1650 J/kg) since it is still affected by the previous dry conditions (point 1). A very rapid reduction of soil water potential down to the value of 23 J/kg occurs between 4 and 9 November (point 2) as a consequence of cumulative rainfall of 77.2 mm in 5 days. Soil water potential continues to decrease until 15 November (point 3), when it reaches the minimum value of 10 J/kg. Then, although air temperature in this season is relatively low, soil water potential slightly increases again in the range between 10 and 22 J/kg until 6 December 2017 (point 4). The observed slight increase in water content is within the measurement uncertainty range. Rainfall that occurred in early December determines the subsequent further increase of water content, until reaching the value of 0.37 m³/m³, while soil water potential keeps almost constant at 9 J/kg, even in the following period between January and March 2018 (point 5 in Fig. 15c). These paths appear first to cross both MDC and MWC and then stand for a long time below and rather far from the MWC. In particular, the behaviour between point 1 and point 3 could be

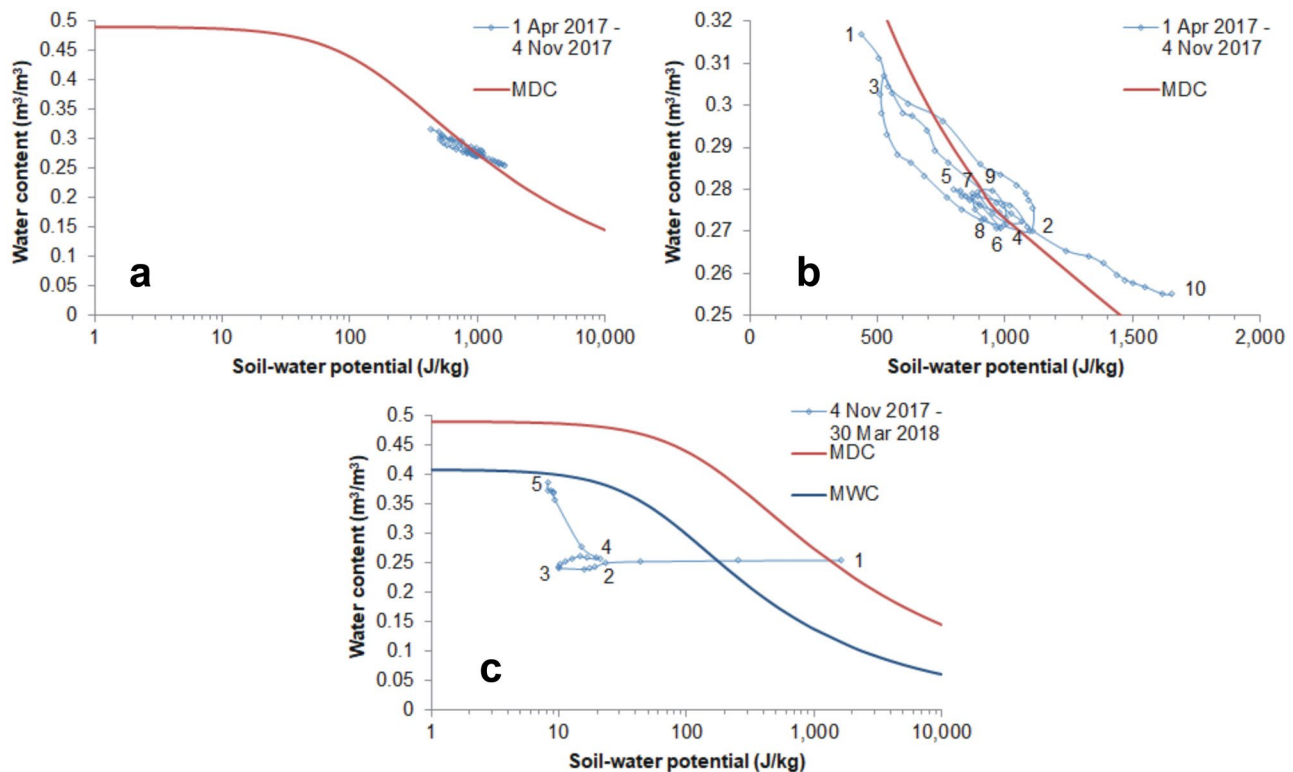


Fig. 15 Costa Cavalieri test site soil at depth of 0.4 m (US). **a** During summer with data reported in logarithmic scale. **b** During summer with data reported in decimal scale. **c** During winter with data reported in logarithmic scale

explained by supposing a gap around the tensiometer tube, due to the presence of some fissures. It could be supposed that some water penetrated through such fissures reaching the tensiometer cap. This has meant that the wetting front takes much more time to reach the TDR probes.

Figure 16a shows the soil behaviour at a depth of 0.6 m during summer 2017. The drying process covers a soil water potential range of about 260 J/kg, starting on 1 April 2017 (point 1) until 8 May 2017 (point 2). Then, rainfall occurred in the first week of May caused a wetting phase until 3 June (point 3) that is characterised by a soil water potential variation between 267 and 197 J/kg. Subsequently, a drying process until 6 September (point 4) is observed. As a consequence of a rain fall of 23.4 mm on 6 September (point 4), soil water potential decreases from 1046 to 42 J/kg on 8 September (point 5), while the water content remains constant around 0.2. This quick drop of water potential in only 2 days at the depth of 0.6 m, not accompanied by any change in water content, does not seem consistent with the hydraulic conductivity of this soil, and so it is likely due to some kind of preferential non-equilibrium flow. The fact that TDR probes do not detect any kind of variation of water content suggests that this is the experimental evidence that a fissure has formed in the soil. Since at Costa Cavalieri test site the soil is prone to shrinkage, a fissure may have

formed around the tensiometer tube during the hot and dry summer (as showed in Fig. 11), and so some water may have penetrated through such a fissure reaching the tensiometer cap, while this did not happen at the TDR probes owing to the different procedure of installation besides the different size and shape of devices.

After 8 September (point 5), soil water potential values increase again up to 1300 J/kg until 4 November (point 6 in Fig. 16a). It could be observed that in this case all hysteretic cycles are mainly between MDC and MWC, unless point 5, which falls below the MWC. The analysis corresponding to the winter season at a depth of 0.6 m is reported in Fig. 16b. At first, between 12 November (point 1) and 19 November (point 2), soil water potential decreases over nearly 1450 J/kg, but water content keeps rather constant between 0.18 and 0.2. This trend is very similar to that observed at 0.4 m, as a consequence of rainfalls that occurred in the first week of November. At the same water content level, a slight increase in soil water potential is then observed until 4 December (point 3). As previously observed at 0.4 m, it could be supposed that the same fissure reached the tensiometer at 0.6 m, the water penetrated through such a fissure much faster than the water has had time to reach the TDR probes. In fact, water content increases much more slowly until attaining 0.4 on 12 December (point 4).

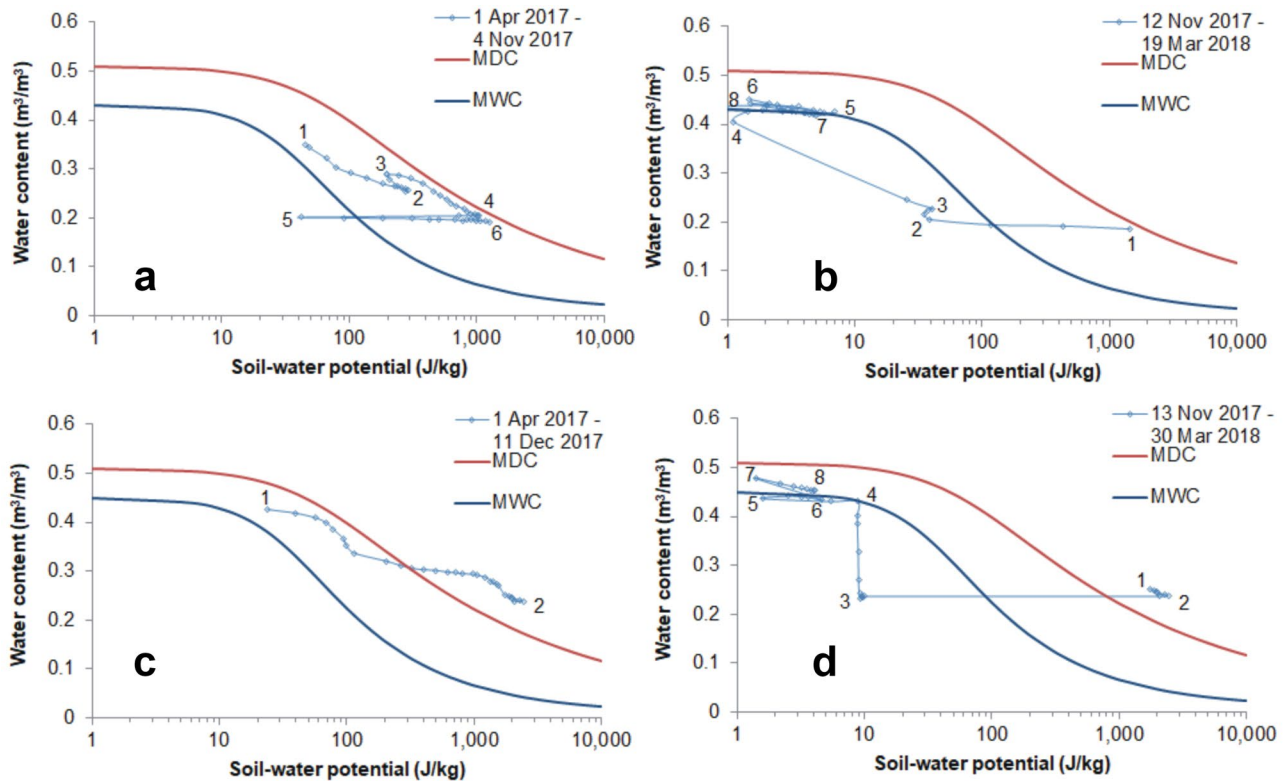


Fig. 16 Costa Cavalieri test site soil at depth of 0.6 m (US) during summer **a** and during winter **b**. Costa Cavalieri test site soil at depth of 0.9 m (US) during summer **c** and during winter **d**

Figure 16b also shows what is observed in the subsequent period, in a narrow range of both soil water potential and water content. A sequence of alternating fluctuations on soil water potential (from point 4 to point 8) could be noticed, although the water content keeps near saturation. Soil water potential ranges over nearly 8 J/kg in each cycle. Although these small cycles are difficult to distinguish graphically, since they involve very small variations in water content; nevertheless, it can be noticed that soil water potential always decreases as consequence of a rainfall event. The last wetting phase begins on 4 March (point 7) and continues until 19 March 2018 (point 8), when water content attains the maximum value of $0.43 \text{ m}^3/\text{m}^3$, which corresponds to complete soil saturation. Meanwhile, soil water potential reaches negative values (not shown in Fig. 16b), which means that pore water pressure becomes positive (up to 4 kPa). This condition corresponds to total saturation and to the formation of a perched water table.

Precipitations occurred during summer 2017 seem not affecting the soil behaviour at a depth of 0.9 m. In fact, a rather uniform drying process that begins on 1 April 2017 and continues until 11 December 2017 can be observed (Fig. 16c). This somehow confirms that preferential flow was just a local issue at the 0.6 m tensiometer; otherwise, something would happen also at 0.9 m after the rainfall event

occurred on 6 September. On the whole period, the water potential ranges between 23 and 2300 J/kg and the drying path appears very close to the MDC (Fig. 16c).

The behaviour at a depth of 0.9 m in the period between 13 November 2017 and 30 March 2018 is reported in Fig. 16d. From 13 November (point 1) to 11 December (point 2), soil water potential still keeps at relatively high levels between 1700 and 2400 J/kg , since it is affected by the previous dry season. Rainfall that occurred in the first week of November does not seem to affect this layer. Instead, as a consequence of the rainfall that occurred in the first week of December (29.4 mm in 4 days), the soil water potential rapidly decreases down to 9.5 J/kg on 12 December, but water content keeps constant at $0.23 \text{ m}^3/\text{m}^3$ (point 3). This quick drop of water potential in only 1 day, with no change in water content, seems to reveal the existence of a further deep fissure at 0.9 m, probably not connected with that at 0.4 and 0.6 m, which allows again a preferential non-equilibrium flow. As at shallower soil layers, even at 0.9 m TDR, probes detect the variation of water content with a certain delay with respect to the tensiometers.

In the following period, while soil water potential remains around the same value of 9.5 J/kg , water content increased up to $0.43 \text{ m}^3/\text{m}^3$ on 17 February 2017 (point 4). During the subsequent period, until 25 February, the wetting phase

continues by following a very different path. Soil water potential decreases from 8.9 down to 1.6 J/kg (point 5), but water content remains almost constant. A short increase in soil water potential follows until 4 March (point 6), then a wetting phase occurs until 19 March (point 7), when water content attains the maximum value of $0.45 \text{ m}^3/\text{m}^3$. Even in this case, soil water potential reaches negative values, i.e. pore-water pressure becomes positive up to 6 kPa (not shown in Fig. 16d). As previously observed, this condition corresponds to the soil saturation, and a perched water table is formed.

Between 19 March (point 7) and 30 March (point 8), no further precipitation occurs and this leads the soil water potential to rise again towards positive values (up to 4 J/kg) and only a slight reduction in water content is observed. These cycles appear very close to the MWC.

The non-equilibrium between soil water potential and water content that has been observed at the three depths of Costa Cavalieri demonstrates how fissures can deeply affect the infiltration process, especially in a soil with a relatively high percentage of clay. In fact, at the Costa Cavalieri test site, field measurements could be interpreted accounting for the presence of deep fissures that form during the dry season, due to shrinkage of clayey soil. This partly confirms what was observed in similar contexts by other authors (Iverson 2000; Zhan et al. 2007; Valentino et al. 2011; Montrasio et al. 2011; Montrasio and Valentino 2016; Chang et al. 2021). Shallow soils contain many pores, channels and fissures, often not connected to each other, which are created by several processes, including weathering and shrinkage-drying cycles. These structures form two preferential pathways for rain infiltration: through the micro-pores in the soil matrix and through the macro-pores. Rainfall infiltrates through the macro-pores much more quickly than through the micro-pores (Shao et al. 2015). Shao et al. (2015) also showed how in case of high intensity rainfall, preferential flows have a negative effect on the slope stability as the majority of rainfall infiltrates into the preferential flow domain, resulting in larger water pressure and a larger failure area.

A similar hydrological behaviour can be observed in loess soils, where the presence of fissures and macro-voids cause a fast response towards rainfall events, with the development of preferential flows and the change in soil hydrological properties (Chang et al. 2021).

Comparison of field measurements with both MDC and MWC at the Costa Cavalieri test site (Figs. 15 and 16) show that in similar conditions, the real hydraulic soil behaviour cannot be modelled appropriately by simply using a main drying and a main wetting SWCC. Models that take into account the existence of hysteretic loops could be more suitable, but even in this case, the transient non-equilibrated conditions may be difficult to reproduce. Furthermore, fissures could be not directly connected to each other. It is

not certain that the deeper, probably sparser and narrower cracks are connected to the more numerous and wider surface cracks.

For both the analysed test sites, soil–water characteristic curves (SWCCs) of the investigated layers were known to be hysteretic (Bordoni et al. 2015), with the main drying path clearly distinct from the main wetting one. However, in the present long-term monitoring, soil response to rainfall appears completely different during the hot season (April–October) than the cold season (November–March) in terms of both soil water potential range and shape of hysteretic cycles. Soil water potential variation in the hot season is wider than in the cold season. Moreover, the pairs of soil water potential and water content measured on site at the same point, depicting the drying–wetting cycle observed in the field, show a series of narrow hysteresis loops, corresponding to different isolated rainy events. A similar behaviour was observed by other authors in different kinds of soils (Papa et al. 2013; Comegna et al. 2016a, b). In most hysteretic loops, the drying path is at a higher position than the wetting path, as typically expected.

It is worth noting that, based on a similar research, Comegna et al. (2021) highlighted how a reliable relationship between volumetric water content and soil water potential in a pyroclastic soil could be affected by different aspects, such as small differences in grain size or porosity, which is also dependent on the installation procedures of the soil around the sensors, and different soil volumes affecting the response of sensors. This has been also observed in the presented results.

Conclusions

The description of long-term monitoring of soil–atmosphere interactions at two test sites in Oltrepò Pavese has given the possibility of achieving a twofold general objective: considering practical aspects of the field research campaign, and deriving useful information on the observed natural phenomena.

Installation and operation of field monitoring devices has been described, also underlining specific choices, in order to infer both potential and shortcomings in the use of the adopted instrumentation. The use of different kinds of sensors to measure soil water potential and water content was found to be generally reliable and satisfactory.

The hydraulic behaviours of two different kinds of soils in the same climatic area, in response to similar weather events, have been compared.

As expected, it has been observed that at both test sites, during the cold season (November–March), after rain events followed by a prolonged dry period, the response of soil

layers down to 0.6 m from ground level is faster than that of the underlying layers. Moreover, the time required to reach a 'dry' state is much longer than that required to reach a saturated condition. This difference affects the observed trends of water content/soil water potential plots. Soil water potential variation in the hot season is wider than in the cold one. Moreover, the pairs of soil water potential and water content measured on site at the same point show a series of narrow hysteresis loops, corresponding to different isolated rainy events, which influence rainwater redistribution especially in the more shallow soil layers. Field monitoring allows also to observe triggering conditions of shallow slope failures, thanks to the measure of soil hydrological parameters immediately before and during a triggering event. In the analysed test sites, triggering mechanism is related to an uprising of soil water potential, from negative values towards zero and, above all, when it grows to positive values. This condition appears rather uncommon throughout most of the year, except for a few days in the cold season, following prolonged rainfall that has allowed water to infiltrate down to an almost impermeable barrier and forms a continuous saturated front.

Besides similar hydrological behaviours, the response in the two test sites is influenced by soil composition and clay content. In particular, higher clay content causes larger fissures and then non-equilibrium relationships between soil water potential and water content can occur, mostly during hot and dry periods.

The above observations suggest that the hydraulic behaviour of an unsaturated soil with respect to rainfall is much more complex than how it is commonly considered for modelling and simulations. First of all, only in some particular cases the shallow soil could be assumed as a 'continuous' mean in which the wet front proceeds from the top towards the deep layers. Even if down to 1.2 m, the soil could be assumed as uniform from a geotechnical point of view; nevertheless, it is not uniform from a hydraulic point of view. The soil between 0 and 1.2 m of depth appears layered, and each layer has its own behaviour. To model appropriately the hydraulic response to weather forcing, at least the SWCC of each layer should be available. However, the use of a single SWCC or of a SWCC composed by a main drying and a main wetting path tend to greatly simplify the behaviour of these layers in unsaturated conditions.

Some physical aspects that could affect soil-atmosphere interaction, such as evapotranspiration, plant uptake and heat fluxes, have not been considered in this work, since the main objective is presenting basic field measurements without any modelling of the observed phenomena. The authors hope to be able to carry out more detailed measurements on the same test sites in the future, so as to supplement the information acquired so far. Moreover, since the test sites are prone to rainfall-induced shallow landslides, whose development

is strongly related to soil hydrological conditions, we will deepen the relationship between the field monitored data and the initiation or evolution of the shallow landslides, integrating also meteorological and hydrological time series with monitoring of displacements, tilting in shallow soil layers and lateral deformations (e.g. Qiao et al. 2020).

Acknowledgements This work has been in the frame of the ANDROMEDA project, which has been supported by Fondazione Cariplo, grant no. 2017-0677. Authors are grateful to Dr. Alice Dallafiora for the support in data processing. The authors thank the anonymous reviewers for their suggestion and contribution to the work.

Funding Open access funding provided by Università degli Studi di Pavia within the CRUI-CARE Agreement.

Open Access This article is licensed under a Creative Commons Attribution 4.0 International License, which permits use, sharing, adaptation, distribution and reproduction in any medium or format, as long as you give appropriate credit to the original author(s) and the source, provide a link to the Creative Commons licence, and indicate if changes were made. The images or other third party material in this article are included in the article's Creative Commons licence, unless indicated otherwise in a credit line to the material. If material is not included in the article's Creative Commons licence and your intended use is not permitted by statutory regulation or exceeds the permitted use, you will need to obtain permission directly from the copyright holder. To view a copy of this licence, visit <http://creativecommons.org/licenses/by/4.0/>.

References

- Ashland FX (2021) Critical shallow and deep hydrologic conditions associated with widespread landslides during a series of storms between February and April 2018 in Pittsburgh and vicinity, western Pennsylvania. *Landslides, USA*. <https://doi.org/10.1007/s10346-021-01665-x>
- Bittelli M, Valentino R, Salvatorelli F, Rossi Pisa P (2012) Monitoring soil-water and displacement conditions leading to landslide occurrence in partially saturated clays. *Geomorphology* 173–174:161–173
- Bordoni M, Bittelli M, Valentino R, Chersich S, Meisina C (2017) Improving the estimation of complete field soil water characteristic curves through field monitoring data. *J Hydrol* 552:283–305
- Bordoni M, Meisina C, Valentino R, Lu N, Bittelli M, Chersich S (2015) Hydrological factors affecting rainfall-induced shallow landslides: from the field monitoring to a simplified slope stability analysis. *Eng Geol* 193:19–37
- Bovolenta R, Iacopino A, Passalacqua R, Federici B (2020) Field measurements of soil water content at shallow depths for landslide monitoring. *Geosci* 10:409
- Campbell GS, van Schilfegaarde J (1981) Use of SI units in soil physics. *Journal of Agronomic Education* 10:73–74
- Chang Z, Huang F, Huang J, Jiang SH, Zhou C, Zhu L (2021) Experimental study of the failure mode and mechanism of loess fill slopes induced by rainfall. *Eng Geol* 280:105941

- Chen P, Ning L, Wei C (2019) General Scanning Hysteresis Model for Soil–Water Retention Curves. *J Geotech Geoenviron Eng* 145(12). [https://doi.org/10.1061/\(ASCE\)GT.1943-5606.0002184](https://doi.org/10.1061/(ASCE)GT.1943-5606.0002184)
- Comegna L, Damiano E, Greco R, Guida A, Olivares L, Picarelli L (2016a) Field hydrological monitoring of a sloping shallow pyroclastic deposit. *Can Geotech J* 53:1–13
- Comegna L, Rianna G, Lee SG, Picarelli L (2016b) Influence of the wetting path on the mechanical response of shallow unsaturated sloping covers. *Comput Geotech* 73:164–169
- Comegna L, Damiano E, Greco R, Olivares L, Picarelli L (2021) The hysteretic response of a shallow pyroclastic deposit. *Earth Syst Sci Data*. <https://doi.org/10.5194/essd-2020-362>
- Crawford MM, Bryson LS (2018) Assessment of active landslides using field electrical measurements. *Eng Geol* 233:146–159
- Crawford MM, Bryson LS, Woolery EW, Wang Z (2018) Using 2-D electrical resistivity imaging for joint geophysical and geotechnical characterization of shallow landslides. *J Appl Geophys* 157:37–46
- Crawford MM, Bryson LS, Woolery EW, Wang Z (2019) Long-term landslide monitoring using soil–water relationships and electrical data to estimate suction stress. *Eng Geol* 251:146–157
- Diamantopoulos E, Iden SC, Durner W (2012) Inverse modelling of dynamic nonequilibrium in water flow with an effective approach. *Water Resour Res* 48:3. <https://doi.org/10.1029/2011WR010717>
- Flint AL, Campbell GS, Ellett KM, Calissendorf C (2002) Calibration and temperature correction of heat dissipation matric potential sensors. *Soil Sci Soc Am J* 66:1439–1445. <https://doi.org/10.2136/sssaj2002.1439>
- Fredlund DG (2019) State of practice for use of the soil–water characteristic curve (SWCC) in geotechnical engineering. *Can Geotech J* 56:1059–1069
- Gasmo JM, Rahardjo H, Leong EC (2000) Infiltration effects on stability of a residual soil slope. *Comput Geotech* 26:145–165
- Godt JW, Schulz WH, Baum RL, Savage WZ (2008) Modelling rainfall conditions for shallow landsliding in Seattle, Washington. In: Baum, RL, Godt, JW, High land, LM (eds.), *Landslides and Engineering Geology of the Seattle, Washington, area*. *Geol Soc Am Rev Eng Geol* 20, pp. 137–152
- Godt JW, Baum RL, Lu N (2009) Landsliding in partially saturated materials. *Geophys Res Lett* 36. <https://doi.org/10.1029/2008GL03599>
- Iverson RM (2000) Landslide triggering by rain infiltration. *Water Resour Res* 36:1897–1910
- Leung AK, Ng CWW (2013a) Seasonal movement and groundwater flow mechanism in an unsaturated saprolitic hillslope. *Landslides* 10(4):455–467
- Leung A, Ng CWW (2013b) Analyses of groundwater flow and plant evapotranspiration in a vegetated soil slope. *Can Geotech J* 50(12):1204–1218
- Leung AK, Sun HW, Millis S, Pappin JW, Ng CWW, Wong HN (2011) Field monitoring of an unsaturated saprolitic hillslope. *Can Geotech J* 48(3):339–353
- Li XS (2005) Modelling of hysteresis response for arbitrary wetting/drying paths. *Comput Geotech* 32:133–137
- Li WC, Lee LM, Cai H, Li HJ, Dai FC, Wang ML (2013) Combined roles of saturated permeability and rainfall characteristics on surficial failure of homogeneous soil slope. *Eng Geol* 153:105–113
- Liang WL (2020) Dynamics of pore water pressure at the soil–bedrock interface recorded during a rainfall-induced shallow landslide in a steep natural forested headwater catchment, Taiwan. *J Hydrol* 587:125003
- Lim TT, Rahardjo H, Chang MF, Fredlund DG (1996) Effect of rainfall in matric suctions on a residual soil slope. *Can Geotech J* 33:618–628
- Lu N, Godt JW (2013) *Hillslope hydrology and stability*. Cambridge University Press, Cambridge, U.K.
- Marino P, Comegna L, Damiano E, Olivares L, Greco R (2020) Monitoring the hydrological balance of a landslide-prone slope covered by pyroclastic deposits over limestone fractured bedrock. *Water* 12:3309
- Mirus BB, Smith JB, Baum RL (2017) Hydrologic impacts of landslide disturbances: implications for remobilization and hazard persistence. *Water Resour Res* 53:8250–8265
- Montrasio L, Valentino R, Losi GL (2011) Rainfall infiltration in a shallow soil: a numerical simulation of the double-porosity effect. *Electr J Geotech Eng* 16(R): 1387–1403
- Montrasio L, Valentino R (2016) Modelling rainfall-induced shallow landslides at different scales using SLIP - Part I, VI Italian Conference of Researchers in Geotechnical Engineering–Geotechnical Engineering in Multidisciplinary Research: from Microscale to Regional Scale, CNRIG2016. *Procedia Engineering* 158:476–481. <https://doi.org/10.1016/j.proeng.2016.08.475>
- Papa R, Pirone M, Nicotera MV, Urciuoli G (2013) Seasonal groundwater regime in an unsaturated pyroclastic slope. *Geotechnique* 63(5):420–426
- Pirone M, Papa R, Nicotera MV, Urciuoli G (2014) Evaluation of the hydraulic hysteresis of unsaturated pyroclastic soils by in situ measurements. *Proc Earth Planet Sci* 9:163–170
- Pirone M, Papa R, Nicotera MV, Urciuoli G (2015a) In situ monitoring of the groundwater field in an unsaturated pyroclastic slope for slope stability evaluation. *Landslides* 12(2):259–276
- Pirone M, Papa R, Nicotera MV, Urciuoli G (2015b) Soil water balance in an unsaturated pyroclastic slope for evaluation of soil hydraulic behaviour and boundary conditions. *J Hydrol* 528:63–83
- Qiao S, Feng C, Yu P, Tan J, Uchimura T, Wang L, Tang J, Shen Q, Xie J (2020). Investigation on surface tilting in the failure process of shallow landslides. *Sensors* 20:2662. <https://doi.org/10.3390/s20092662>
- Rahardjo H, Lee TT, Leong EC, Rezaur RB (2005) Response of a residual soil slope to rainfall. *Can Geotech J* 42:340–351
- Rahardjo H, Leong EC, Rezaur RB (2008) Effect of antecedent rainfall on pore-water pressure distribution characteristics in residual soil slopes under tropical rainfall. *Hydrol Processes* 22: 506–523
- Rahardjo H, Santoso VA, Leong EC, Ng YS, Hua CJ (2011) Numerical analyses and monitoring performance of residual soil slopes. *Soils Found* 51(3):471–482
- Rianna G, Pagano L, Urciuoli G (2014) Investigation of soil–atmosphere interaction in pyroclastic soils. *J Hydrol* 510:480–492
- Rogers JS, Klute A (1971) The hydraulic conductivity–water content relationship during non-steady flow through a sand column. *Soil Sci Soc Am J* 35(5):695–700
- Ross P, Smettem KRJ (2000) A simple treatment of physical nonequilibrium water flow in soil. *Soil Sci Soc Am J* 64:1926–1930
- Shao W, Bogaard TA, Bakker M, Greco R (2015) Quantification of the influence of preferential flow on slope stability using a numerical modelling approach. *Hydrol Earth Syst Sci* 19: 2197–2212. <http://www.hydrol-earth-syst-sci.net/19/2197/2015/doi:10.5194/hess-19-2197-2015>
- Simunek J, Jarvis NJ, Van Genuchten MT, Gardenas A (2003) Review and comparison of models for describing non-equilibrium and preferential flow and transport in the vadose zone. *J Hydrol* 272:14–35
- Smethurst JA, Clarke D, Powrie D (2012) Factors controlling the seasonal variation in soil water content and pore-water pressures within a lightly vegetated clay slope. *Geotechnique* 62(5):429–446. <https://doi.org/10.1680/geot.10.P.097>
- Springman SM, Thielen A, Kienzler P, Friedel S (2013) A long-term field study for the investigation of rainfall-induced landslides. *Geotechnique* 14:1177–1193. <https://doi.org/10.1680/geot.11.P.142>

- Tami D, Rahardjo H, Leong EC (2004) Effects of hysteresis on steady-state infiltration in unsaturated slopes. *J Geotech Geoenviron Eng* 130(9):956–966
- Tang YM, Xue Q, Li ZG, Feng W (2015) Three modes of rainfall infiltration inducing loess landslide. *Nat Hazards* 79:137–150
- Tohari A, Nishigaki M, Komatsu M (2007) Laboratory rainfall-induced slope failure with moisture content measurement. *J Geotech Geoenviron Eng* 133(5):575–587
- Valentino R, Montrasio L, Losi GL, Bittelli M (2011) An empirical model for the evaluation of the degree of saturation of shallow soils in relation to rainfalls. *Can Geotech J* 48:795–809. <https://doi.org/10.1139/T10-098>
- Vercesi P, Scagni G (1984) Osservazioni sui depositi conglomeratici dello sperone collinare di Stradella. *Rend Soc Geol Ital* 7- 23–26 (in Italian)
- Vogel HJ, Weller U, Ippisch O (2010) Non-equilibrium in soil hydraulic modelling. *J Hydrol* 393:20–28
- Watakabe T, Matsushi Y (2019) Lithological controls on hydrological processes that trigger shallow and slides: Observations from granite and hornfels hillslopes in Hiroshima, Japan. *CATENA* 180:55–68
- Wei X, Fan W, Chai X, Cao Y, Nan Y (2020) Field and numerical investigations on triggering mechanism in typical rainfall-induced shallow landslides: a case study in the Ren River catchment, China. *Nat Haz* 103:2145–2170
- Yang C, Sheng D, Carter JP (2012) Effect of hydraulic hysteresis on seepage analysis for unsaturated soils. *Comput Geotech* 41:36–56
- Zhan TLT, Ng CWW, Fredlund DG (2006) Instrumentation of an unsaturated expansive soil slope. *Geotech Test J* 30(2):1–11
- Zhan TLT, Ng CWW, Fredlund DG (2007) Field study of rainfall infiltration into a grassed unsaturated expansive soil slope. *Can Geotech J* 44:392–408